1-1-2004

Three-dimensional CFD simulations of natural and forced convection solar domestic water heating systems

Sachin Sudhakar Deshmukh
University of Nevada, Las Vegas

NOTE TO USERS

3 D CFD SIMULATIONS OF NATURAL AND FORCED CONVECTION SOLAR DOMESTIC WATER HEATING SYSTEMS

by

Sachin Sudhakar Deshmukh

Bachelor of Engineering
Amravati University, India
1999

A thesis submitted in partial fulfillment
of the requirements for the

Master of Science Degree in Mechanical Engineering
Department of Mechanical Engineering
Howard R. Hughes College of Engineering

Graduate College
University of Nevada, Las Vegas
December 2004

UNLV
UNIVERSITY OF NEVADA LAS VEGAS

Thesis Approval

The Graduate College
University of Nevada, Las Vegas

December 15, 2004

The Thesis prepared by

Sachin S. Deshmukh

Entitled

3 D CFD Simulations of Natural and Forced Convection Solar Domestic Water Heating Systems

is approved in partial fulfillment of the requirements for the degree of

Master of Science in Mechanical Engineering

Examination Committee Chair

Dean of the Graduate College

Examination Committee Member

Examination Committee Member

Graduate College Faculty Representative

ABSTRACT

3 D CFD Simulations of natural and forced convection solar domestic water heating systems

by

Sachin Sudhakar Deshmukh

Dr. Samir Moujaes, Examination Committee Chair
Professor, Mechanical Engineering
University of Nevada, Las Vegas

The objective of the thesis is to study the thermal performance of the open loop natural convection and closed loop forced convection solar water heating system. The 3 dimensional (3D) numerical models were made in the Computer aided design (CAD) package and were simulated for the 12 hours of day time. Analysis was performed using the Computational fluid dynamics (CFD) software package Star-CD. The physical system of natural convection can be used for the purpose of heating domestic hot water without the use of a circulating pump. The closed loop forced circulation system is simulated to study the numerical behavior of the system with respect to time which can further predict the performance of the system when it is connected to the water mains for actual residential applications.

The solar water heater that is being simulated is a truly flat surface collector where the water is allowed to flow in a thin rectangular channel cross-section. The CFD simulations are performed to predict the velocity and temperature of the water in these

systems. An accurate relationship between density and temperature of water is implemented for the purpose of predicting the buoyancy effects in the natural convection case. It is felt that the continuous rectangular cross-section chosen will tend to reduce the overall heat losses from the collector hence increasing the thermal performance as the average collector surface temperature will be reduced compared to a typical plate and tube solar collector.

The open loop system is defined as the system in which the solar water heater is connected to the water mains. The cold water from the tap can be fed to the system and the hot water can be extracted from the system for utilization. The closed loop system is defined as the system in which water is circulated inside the system itself and there is no feeding or extraction of water from the system.

TABLE OF CONTENTS

LIST OF FIGURES

ACKNOWLEDGEMENTS

I would like to acknowledge the help and esteemed guidance of the Project Investigator and my academic advisor Dr. Samir Moujaes for providing supervision and assistance with every step of the work.

I would like to thank Dr. William Culbreth, Dr. Mohamed Trabia and Dr. Samaan Ladkany for there support.

I would like to thank the Department of Mechanical Engineering for funding the project for purchase of extra licenses of Star CD.

Support from the Voss Lytle and Jaime E. Combariza from NSCEE is greatly appreciated.

CHAPTER 1

INTRODUCTION AND BACKGROUND

1.0. Solar Domestic Water Heating Systems

Solar domestic hot water systems are widely used in countries like Australia, Israel and Jordan, and have tremendous potential in other developing countries [1]. These systems operating costs is negligible as compared to conventional hot water systems [2]. The initial cost of these systems being too high is one of the main stumbling blocks in the more common usage of these systems.

1.1. Classification of solar water heating systems

1.1.1. Natural circulation solar water heaters

In natural circulation solar water heaters the fluid is circulated by natural convection. The sketch of conventional natural circulation solar water heater is shown in figure 1. The collector absorbs the heat from the sun. The thermal energy absorbed in the collector fluid is then transferred to the circulating fluid, which creates the fluid density difference between the collector fluid and fluid inside the storage tank. This density difference results in a buoyancy effect and hence circulation of fluid inside the solar water heater. During the night there is a possibility of flow reversal in solar collector i.e. water enters through the top of the collector and leaves from the bottom of collector, hence losing the heat to the atmosphere. Thus a check valve is provided in order to

prevent this effect of nocturnal radiation on the solar water heating systems. The most important parameters that controls the flow rate in a natural circulation solar water heater is the location of storage tank above the collector and pipe sizing and the amount of radiation absorbed by the collector, which varies throughout the day and year.

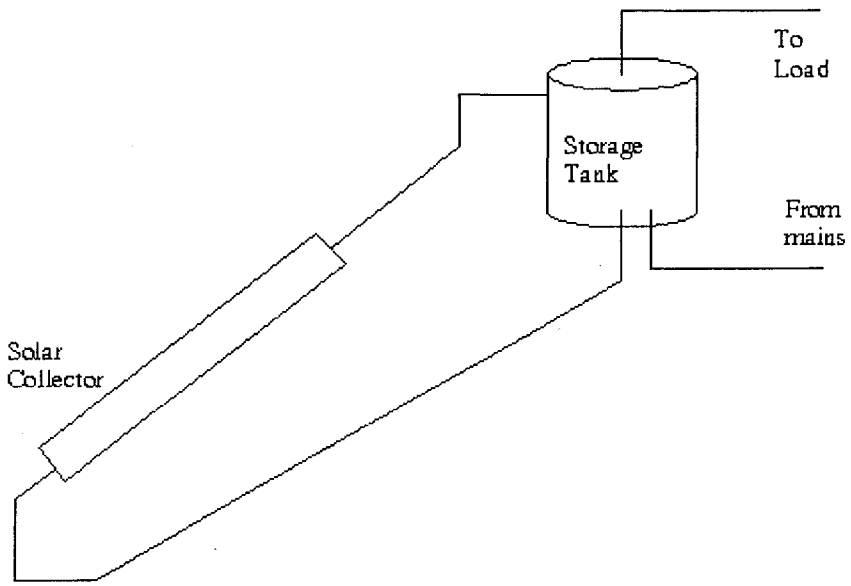

Figure 1: Direct type Natural circulation solar water heater

1.1.2. Forced circulation solar water heater

The forced circulation solar water heater uses a pump for the circulation of fluid in the solar water heater. A pump is normally controlled by a differential temperature-sensing controller that turns on the pump on when the collector outlet temperature is greater than the temperature in the bottom of the tank [2]. Thus the flow inside the forced circulation can be either mixed convection or forced convection depending on the Reynolds number at which the system is operating. Thus the pump increases the initial

cost as well as the operating cost of the system. The sketch of forced circulation solar water heater is shown in figure 2.

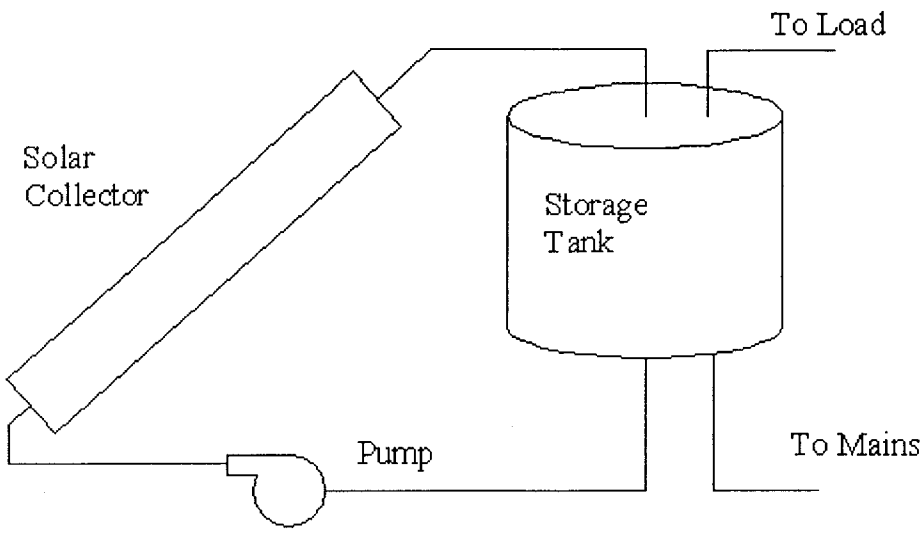

Figure 2: Direct type Forced circulation solar water heater

Solar domestic water heating systems can also be classified as direct or indirect type. In direct type systems the heat is transferred from the collector to domestic water directly. The system in figures 1 and 2 are examples of direct type solar water heaters. In the indirect type the heat is transferred from the collector to the water using an intermediate fluid and an indirect heat exchanger. The indirect type systems are used generally in geographical regions with cold weather conditions. One such intermediate fluid is a mixture of water and ethylene glycol, which can operate in cold temperature without freezing depending on the concentration of ethylene glycol. The indirect type solar water heating systems is shown in figure 3.

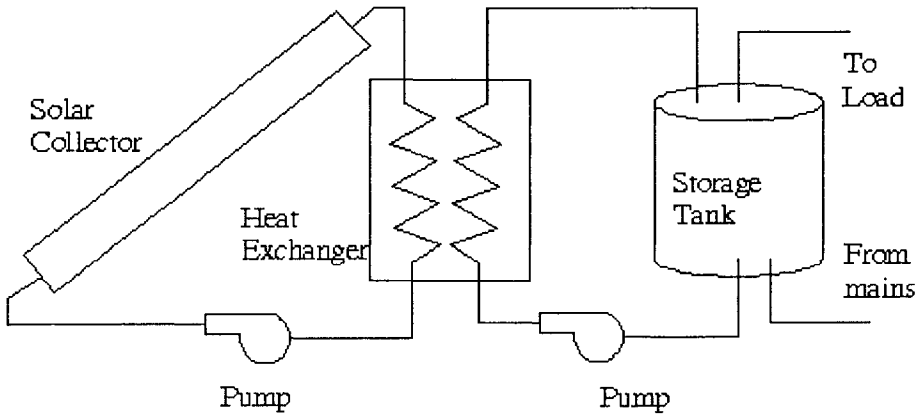

Figure 3: Indirect type solar water heating system

Several numerical and experimental studies have been performed on both natural (thermosyphon) and forced circulation type of solar water heating systems which are briefly discussed below.

The numerical studies consist of developing a model of solar water heating system and conducting the simulations. It was observed that major work has been done using TRNSYS simulation program in the past, some of which are given in brief as follows:

A study was conducted using TRNSYS simulation program for Los Angeles for comprehensive assessment of the impact of most of the design parameters on efficiency and solar fraction to provide guidance on the "optimum" value for each with an objective to maximize annual performance of a domestic thermosyphon solar water system. [4].

A study was conducted using TRNSYS simulation program in which a model of thermosyphon solar water heater was developed to determine the instantaneous collector efficiency as a function of the time of day and correlated with the thermosyphonic-flow

rate of water and the temperature difference between the water at the collector's inlet and outlet. The model was also used to predict the monthly and yearly solar contribution of the system for two different load profiles. [5].

A study was conducted using TRNSYS program in which model of forced circulation solar hot water system was used to correlate the performance and cost effectiveness of the system with a number of key design criteria (e.g. the collector to consumer factor (FCC) and the collector to load factor (FCL)) with an objective to optimize the design criteria of solar hot water (SHW) systems intended for residential hotel applications. [3].

A study of thermosyphon systems was done to determine collector flow rates and thermal stratification in storage tanks, to assess how these flow rates relate to those used in pumped systems with various control strategies, and develop a design method for thermosyphon system based on the equivalent flow rates for pumped system. Thermal stratification in the storage tank was accounted for through use of a modified collector heat loss coefficient. Comparison was made between the annual solar fraction predicted by design method and TRNSYS simulations for a wide range of thermosyphon solar DHW systems. [1].

The authors developed a computationally efficient high-level model for simulating indirect thermosyphon solar energy water heaters to study the characteristics of hot water stored under steady state and real operating conditions. The results indicated that the degree of stratification in a hot water store was correlated with the ratio of collector to load volume flow [6].

The authors derived a more general and realistic model in which the loss of heat through the storage tank is considered and the variation of solar radiation, ambient air temperature and temperature of the cold feed water was taken into account. A transient analysis of forced circulation solar water heating system with and without heat exchangers in the collector loop and storage tank was presented. Exact solutions of different cases were presented and analyzed [7]

Authors presented details of experimental observations of temperature and flow distribution in a natural circulation solar water heating system and its comparison with the theoretical models and showed the measured profile of the absorber temperature near the riser tubes conforms well to the theoretical models. The mean absorber plate temperature and mean fluid temperature during a day has been estimated and compared with theoretical models. Measurements of glass temperature were also carried out [8].

An experimental study was conducted by authors to compare the performance of natural and forced circulation domestic solar water heaters. The main parameters calculated are top, back, and overall coefficients, the heat removal factor, the efficiency factor the useful energy gain and instantaneous efficiency. [9]

A test conducted on built-in solar water heater which was tested both experimentally and theoretically under three different operation modes namely; no flow, continuous flow and intermittent flow. It was found that the average efficiency (η) of the system is of maximum value under the continuous flow condition, while it has a maximum hourly efficiency under the intermittent flow condition [10].

Authors conducted an analytical experimental investigation into the temperature field inside the hot water storage tank of a solar collector on a transient two-dimensional

semi-infinite cylindrical length model with time-and-space boundary conditions dependency was selected. Conduction and convection heat transfer modes in the axial direction together in conduction in radial direction were neglected. Temperature profiles in the axial direction of a cylindrical storage tank were assumed to be linear [11].

Author presented mathematical model for the transient conjugated behavior of hot water storage tank having finite wall thickness and obtained closed form solution for the temperature field within the tank while considering the axial conduction of heat in both fluid and solid wall and the heat capacity of the solid wall. Results showed that finite wall thickness tends to decrease the thermal stratification within the tank and this effect becomes less apparent at high Peclet numbers [12].

Besides this several other experimental and numerical research work on solar water heating systems were done by Adnan M Shariah and A. Ecevit [13], Eng. Malek Kabariti and Eng. Yaser Mowafi [14], I.M. Michaelides and D.R. Wilson [15], Soteries A. Kalogirou, Sofia Panteliou and Argiris Dentsoras [16], B. Norton, P.C. Eames and S.N.G. Lo [17], M. Altamush Siddiqui [18]. Also from literature only one research paper was found in which the CFD program (FLUENT) and a solar simulator, for designing a solar water heater [19]. CFD transient simulations were carried out by him using small time step of 10 seconds and a set of body fitted computational grids (1770*4740 nodes). FLUENT results were the verified against indoor testing employing a solar simulator. He mentioned it that it took a long time for him to get the results.

1.2. Significance of work

Residential hot water use represents a large proportion of residential energy use. Thus the residential energy usage can be reduced significantly if solar water heating systems could be effectively used for water heating. Till now, the initial cost of the solar water heating systems has been the major stumbling block for the usage of solar water heater [2]. Most of the studies carried out in past on solar water heating systems are either experimental or numerical which involves significantly high costs. Also the majority of past studies were conducted on plate and tube type of collector where the major heat will transfers from the part of the flat plate between the tubes to the water. The water flow through a flat cross sectional channel instead of flat plate and tube type of arrangement can reduce the heat losses from the solar collector. In two decades CFD has emerged as a powerful simulation technique for the cost effective study of various heat transfer and fluid flow problems with reasonable accuracy as compared to other approaches, but the study of solar water heating systems using this technique was very rare.

Hence the present study using CFD of three dimensional model of natural convection open loop and forced convection closed loop solar water heating system will add to the literature and potential physical insight in this area. This study will concentrate on a natural convection open loop and forced convection closed loop system simulation. The solar collector studied is of truly flat shape, which would increase the amount of heat transfer from collector to the water as compared to flat plate and tube type design. This study can be extended further to optimize different parameters and materials for the optimum design and cost reduction of both natural and forced convection solar water

heaters and thereby would further help to increasing the usage of solar water heaters which are still not that popular due to high initial costs.

CHAPTER 2

MODEL DESCRIPTION AND NUMERICAL METHOD

This chapter provides information on the working theory behind the simulation package used to model the solar water heating systems considered for simulations. The chapter is split into two subchapters. The first part provides a detailed description of the physical model of the solar water heating systems used for the present study. The second subchapter presents the details of numerical model that were used for the present study.

2.0. Model Description

The physical model of the solar water heater used for the CFD simulation consists of flat surface solar collector and water reservoir connected by a piping system. The solar collector considered here is of truly flat shape rather than a conventional fin and tube type collector. The fin and tube type collector usually exhibit larger heat loss along the upper face of the collector than flat ones because the average temperature on the flat surfaces is lower. Also as the pipes are connected to the flat plate through brazing the amount of heat transferred to water depends on the conductivity and quality of the brazing. Hence in order to maximize heat transfer from collector to water an alternative design of truly flat shaped collector shown in figure 4 (dimensions shown in figures 6 and 7) is used for CFD simulation where all the heat collected by collector will be directly conducted to water flowing below it.

The solar collector was considered to be south facing with an inclination of solar collector (34.759 Deg) from the horizontal was considered for the Las Vegas, NV for the month of June [2]. The flat plate collector is connected to pipes with a conical section shown in figure 4 (dimensions shown in figures 6 and 7). The conical section is designed to ensure that the water flows evenly through the cross section area of solar collector and back into the pipes from top of the collector. The pipes are further connected to the water reservoir from where water can be tapped for usage depending on load.

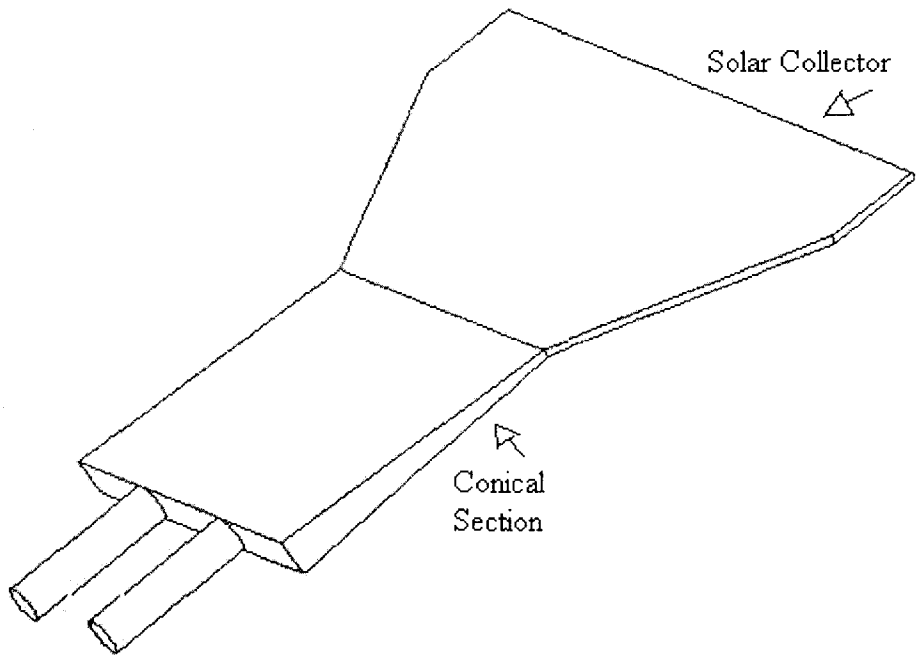

Figure 4: Conical Section that connects the solar collector and pipe

2.0.1. Natural convection open loop solar water heating system simulation

The open loop system was used to perform simulations for natural convection solar water heating system (figure 5) to make it realistic for residential applications. The top surface of the solar collector receives the heat from the sun. No glass cover or metal

surface is simulated in this effort. A certain amount of solar heat flux is imposed as input on the upper most surface of the collector. This heat is then convected to the water flowing in the rectangular channel. The sides of the collector, which exhibit a relatively small area, are assumed to be adiabatic as is the backside of the collector.

The heat gained by water as it flows results in the change of density of water. It is this density difference due to which the water flows from collector to the reservoir and back. As the time increases the closed loop of water flow is set up between the collector and reservoir which results in rise of temperature of water inside the reservoir. In the effort to make this system realistic for residential application the simulation was programmed so that water was tapped at different times a day namely interval I and 2. The schedule for interval for tapping hot water from reservoir is: Interval 1- 20 min from 13:00 pm to 13:20 pm, Interval 2- 20 min from 17:00 pm to 17:20 pm. The inlet is introduced from the bottom and outlet from the top to tap into the hottest water layers of the reservoir. The dimensions for this system is same as shown in figures 6 and 7 except that the inlet and outlet pipes are introduced at the top and bottom of the water reservoir.

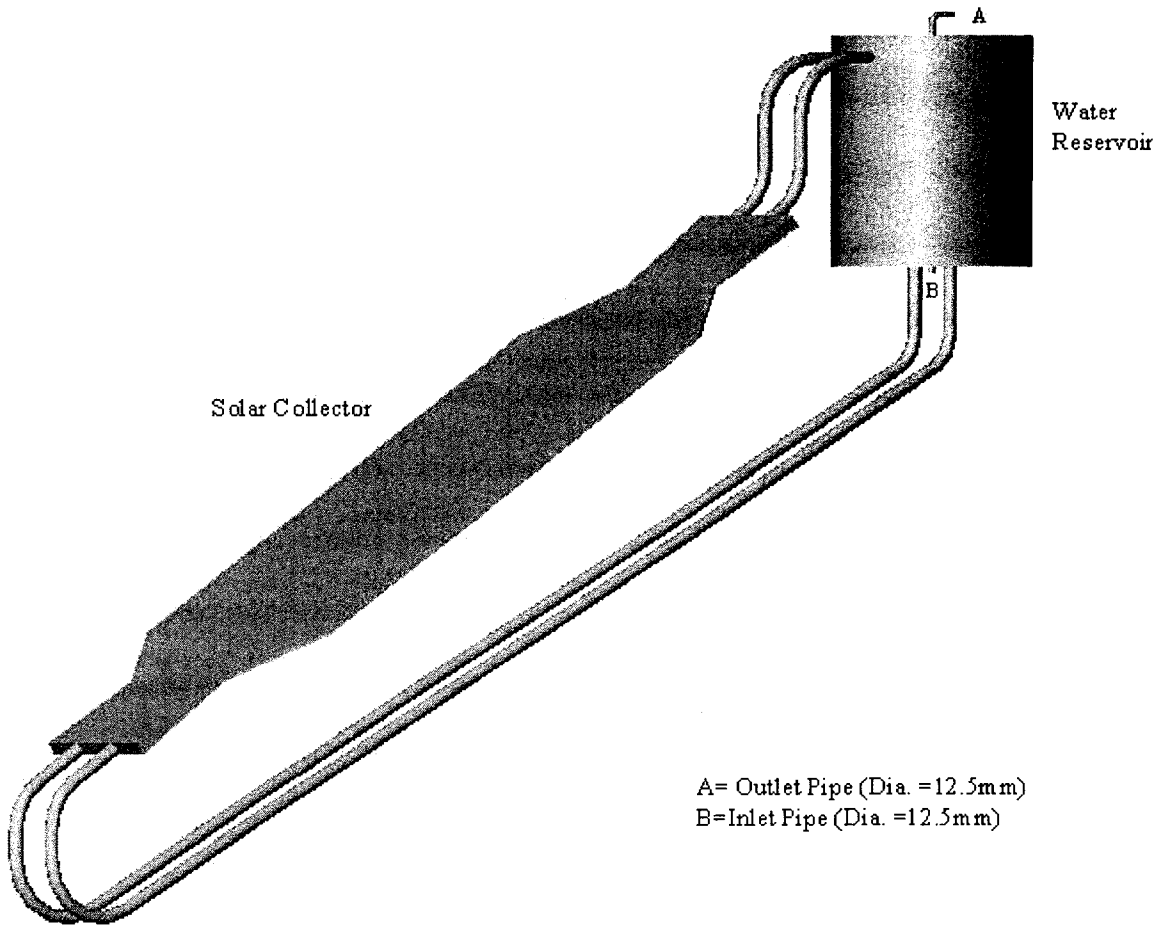

Figure 5: Natural convection open loop solar water heater used for CFD simulations

2.0.2 Forced convection closed loop solar water heating system simulation

A closed loop system simulations for the forced convection solar water heating system was performed. This meant that no make up water was used in the simulation and no hot water was tapped from the system. This is not how the forced circulation solar system is run on a daily average, but the simulation results are useful to shed some light on the general performance of the system. It also gives some preliminary numerical values of what to expect when a more realistic system is studied.

The figures 6 and 7 show the diagram and dimensions of the closed loop system. This study can help further to simulate the forced convection solar water heater for different Reynolds number and there performance comparison.

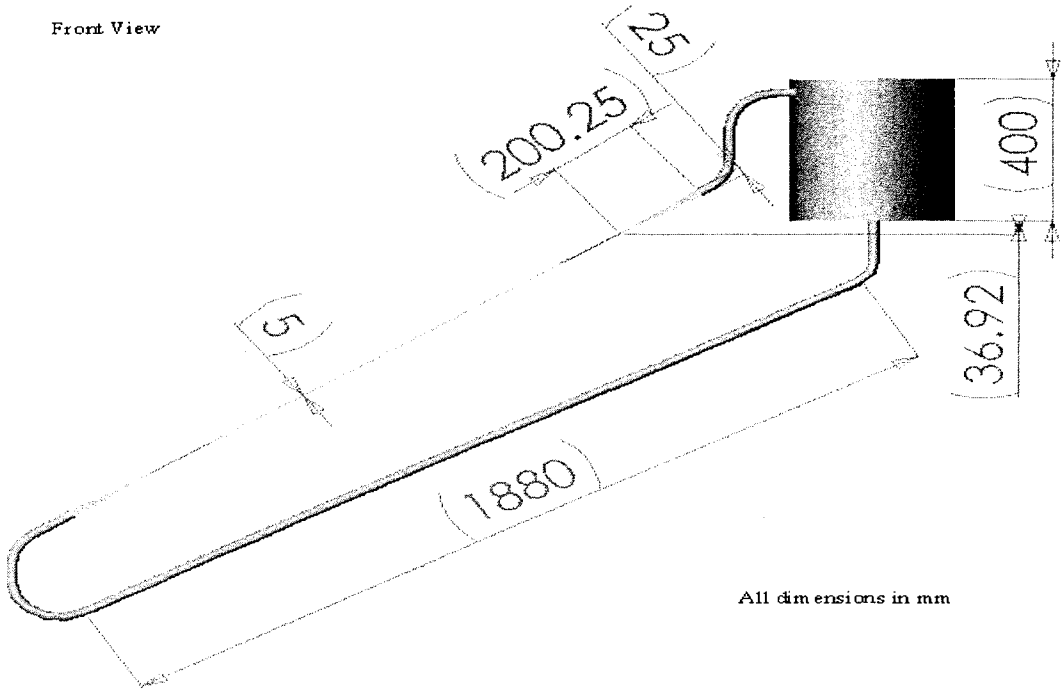

Figure 6: Front view of closed loop solar water heating system with dimensions

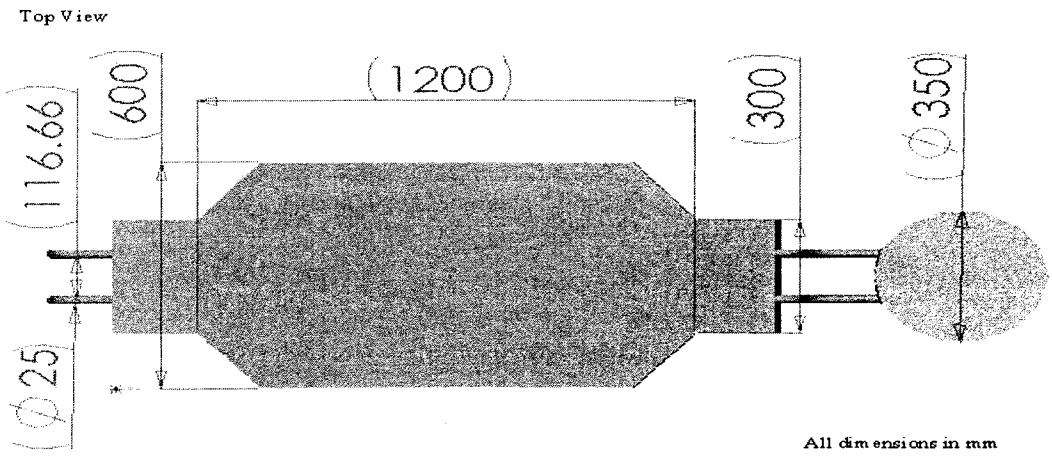

Figure 7: Top view of closed loop solar water heating system with dimensions

2.1. Introduction to Computational Fluid Dynamics (CFD) Simulations System

A STAR-CD program is used for this study. The code comprises of the main analysis code STAR (Simulation of Turbulence in Attributed Regions), and the preprocessor and post-processor code, PROSTAR. STAR-CD is a powerful CFD tool for thermo-fluids analysis and has been designed for use in a Computer Aided Engineering environment. It is a finite volume code, developed for the calculation of fluid flow, heat and mass transfer and chemical reaction in industrial and environmental applications. Its main attributes include:

- A self-contained, fully-integrated and user-friendly program suite comprising pre-processing, analysis and post-processing facilities
- A general geometry-modeling capability that renders the code applicable to the complex shapes often encountered in industrial applications
- Extensive facilities for automatic meshing of complex geometries, either through built-in tools or through interfaces to external mesh generators such as SAMMTM and ICEM CFD TetraTM.
- Built-in models of an extensive and continually expanding range of flow phenomena, including transients, compressibility, turbulence, heat transfer, mass transfer, chemical reaction and multi-phase flow
- Fast and robust computer solution techniques that enhance reliability and reduce computing overheads
- Easy-to-use facilities for setting up and running very large CFD models using state-of-the-art parallel computing techniques

- Built-in links with popular proprietary CAD/CAE systems, including PATRANTM, IDEASTM and ANSYSTM

STAR, written in FORTRAN 77 and C, operates by solving the governing differential equations of flow physics by numerical means on a computational mesh. PROSTAR is an interactive, command-driven, combined pre-processor and postprocessor whose main functions include geometry modeling and mesh generation, problem specification, results manipulation and display, file control, and links to external CAD/CAE systems. The governing equations used by STAR-CD [20] are given below:

The mass and momentum conservation equations solved by STAR-CD for general incompressible fluid flows and a moving coordinate frame ('Navier-Stokes' equations) are, in Cartesian tensor notation:

Mass conservation

$$\frac{1}{\sqrt{g}}\frac{\partial(\sqrt{g}\rho)}{\partial t}+\frac{\partial(\rho\tilde{u}_j)}{\partial x_j}=s_m \qquad (1)$$

Momentum conservation

$$\frac{1}{\sqrt{g}}\frac{\partial(\sqrt{g}\rho u_i)}{\partial t}+\frac{\partial(\rho\tilde{u}_j u_i-\tau_{ij})}{\partial x_j}=-\frac{\partial p}{\partial x_i}+s_i \qquad (2)$$

Where t: time

$x\,i$: Cartesian coordinate (i=1, 2, 3)

ui: absolute fluid velocity component in direction *xi*

$\tilde{u}_j$: *uj-ucj*, relative velocity between fluid and local (moving)coordinate frame that moves with velocity *ucj*

p: peizometric pressure= *ps* -*ρogmxm* , where *ps* is static pressure, *ρo* is reference density, the *gm* are gravitational field components and the *xm* are coordinates from a datum, where *ρo* is defined

ρ : density

τ ij: stress tensor components

sm: mass source

si: momentum source components

$\sqrt{g}$: determinant of metric tensor and repeated subscripts denote summation.

The specialization of the above equations to a particular class of flow involves:

- Application of ensemble or time averaging if the flow is turbulent
- Specification of a constitutive relation connecting the components of the stress tensor τ_{ij} to the velocity gradients
- Specifications of the 'source', *si*, which represents the sum of the body and other external forces, if present.

In case of laminar flows, STAR-CD is applicable to Newtonian fluids that obey the following constitutive relation:

$$\tau_{ij} = 2\mu s_{ij} - \frac{2}{3}\mu \frac{\partial u_k}{\partial x_k}\delta_{ij} \qquad (3)$$

where μ is the molecular dynamic fluid viscosity and δij, 'Kronecker delta', is unity when $i=j$ and zero otherwise. s_{ij}, the rate of strain tensor, is given by:

$$s_{ij} = \frac{1}{2}\left(\frac{\partial u_i}{\partial x_j} + \frac{\partial u_j}{\partial x_i}\right) \qquad (4)$$

For turbulent flows, u_i, p and other dependent variables, including τ_{ij}, assume their ensemble averaged values (equivalent to time averages for steady-state situations) giving, or equation 28:

$$\tau_{ij} = 2\mu s_{ij} - \frac{2}{3}\mu \frac{\partial u_k}{\partial x_k}\delta_{ij} - \overline{\rho u_i' u_j'} \qquad (5)$$

where the u' are fluctuations about the ensemble average velocity and the over bar denotes the ensemble averaging process. The rightmost term in the above equation represents the additional Reynolds stresses due to turbulent motion. These are linked to the mean velocity field via the turbulence models.

Heat transfer in STAR-CD is implemented through the following general form of the enthalpy conservation equation for a fluid mixture:

$$\frac{1}{\sqrt{g}}\frac{\partial}{\partial t}(\sqrt{g}\rho h) + \frac{\partial}{\partial x_j}(\rho \tilde{u}_j h - F_{h,j}) = \frac{1}{\sqrt{g}}\frac{\partial}{\partial t}(\sqrt{g}p) + \tilde{u}_j \frac{\partial p}{\partial x_j} + \tau_{ij}\frac{\partial u_i}{\partial x_j} + s_h \qquad (6)$$

Here, h is the static enthalpy, defined by:

$$h \equiv \bar{c}_p T - c_p^0 T_0 \qquad (7)$$

and T: absolute temperature

$\bar{c}_p$: Mean constant pressure specific heat at temperature T

c_p^o: reference specific heat at temperature T_0

s_h: energy source

h_t: thermal enthalpy

It should be noted that the static enthalpy h is defined as the sum of the thermal and chemical components, the latter being excluded as it is not pertinent to the analysis here.

The governing equation for thermal enthalpy is given by:

$$\frac{1}{\sqrt{g}}\frac{\partial}{\partial t}(\sqrt{g}\rho h_t)+\frac{\partial}{\partial x_j}(\rho\tilde{u}_j h_t - F_{h_t,j}) = \frac{1}{\sqrt{g}}\frac{\partial}{\partial t}(\sqrt{g}p)+\tilde{u}_j\frac{\partial}{\partial x_j}+\tau_{ij}\frac{\partial u_i}{\partial x_j}+s_h \quad (8)$$

Here, h_t is the thermal enthalpy, defined by

$$h_t \equiv \bar{c}_p T - c_p^0 T_0 \quad (9)$$

and $F_{ht,j}$: diffusional thermal energy flux in direction x_j

A governing equation for total thermal enthalpy (H) may be formed by summing an equation for mechanical energy conservation and static enthalpy equation:

$$\frac{1}{\sqrt{g}}\frac{\partial}{\partial t}(\sqrt{g}\rho H)+\frac{\partial}{\partial x_j}(\rho\tilde{u}_j H - F_{h,j} - u_i\tau_{ij}) = \frac{1}{\sqrt{g}}\frac{\partial}{\partial t}(\sqrt{g}p)-\frac{\partial}{\partial x_j}(u_{c_i}p)+s_i u_i+s_h \quad (10)$$

where, $H=(1/2)\,ui + h$ (11)

2.2. Numerical Model

2.2.1. Natural convection open loop solar water-heating system simulation

The numerical model for the solar water heater is 3-D with total number of nodes as 323407 for open loop system. The type of cell used was tetrahedral with a cell size of approximately 2.5 mm for inlet and outlet pipe, 5 mm for the solar collector and the piping system and 16 mm for reservoir. The 3-D model was made in a CAD program and was meshed in the Star CD. Figure 8 and 9 shows the mesh generated by Star CD for the CFD simulations. The time step used for simulations was 15 seconds and the simulations were run for real-time from 0700am to 1900pm.

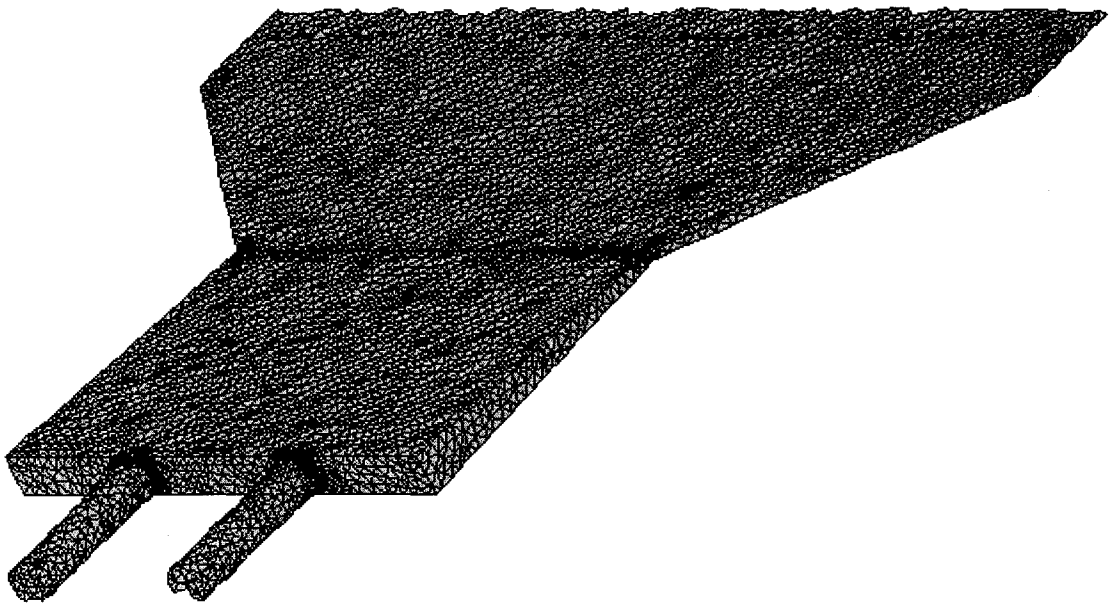

Figure 8: Mesh for pipe, conical section and solar collector used for CFD simulations

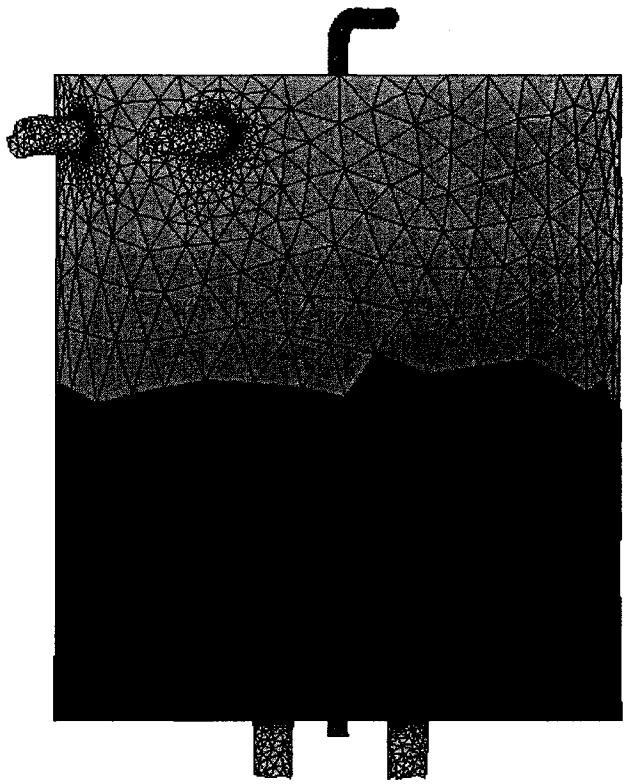

Figure 9: Mesh for reservoir, inlet pipe and outlet pipe used for CFD simulations

The boundary condition for different sections of system is as follows:

1. Solar collector: The top surface of the solar collector was supplied with a boundary condition of heat flux with respect to time (figure 10) that will be acting as solar insolation [21].

2. Pipes, conical section, water reservoir and for bottom and side parts of the collector are supplied with adiabatic boundary condition.

3. The inlet pipe is forced with the flow rate of 3 GPM, which simulates the hot water usage twice a day as shown in figure 11 schedule.

4. Outlet pipe is supplied with boundary condition to satisfy continuity equation.

The thermal performance of the solar water heater was obtained by simulation from 0700am to 0700pm.

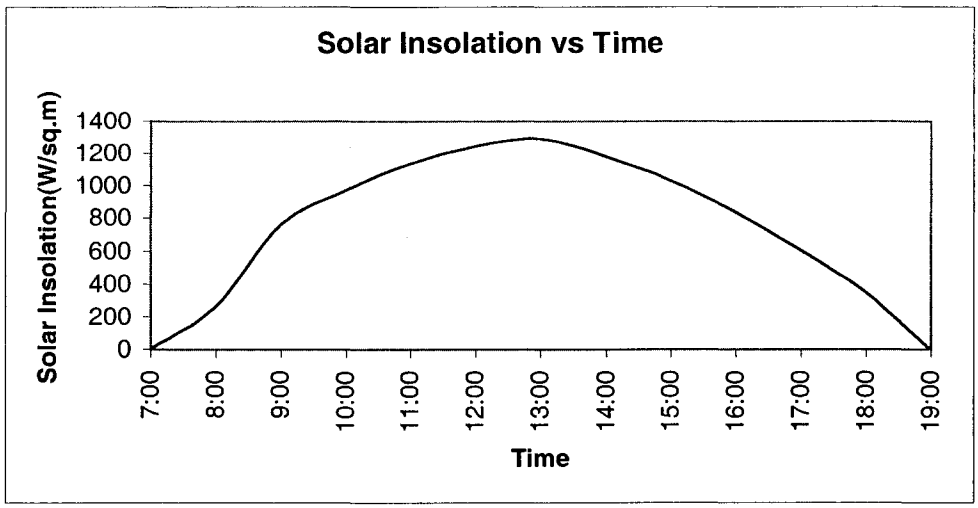

Figure 10: Solar insolation used for CFD simulation from 0700 to 1900

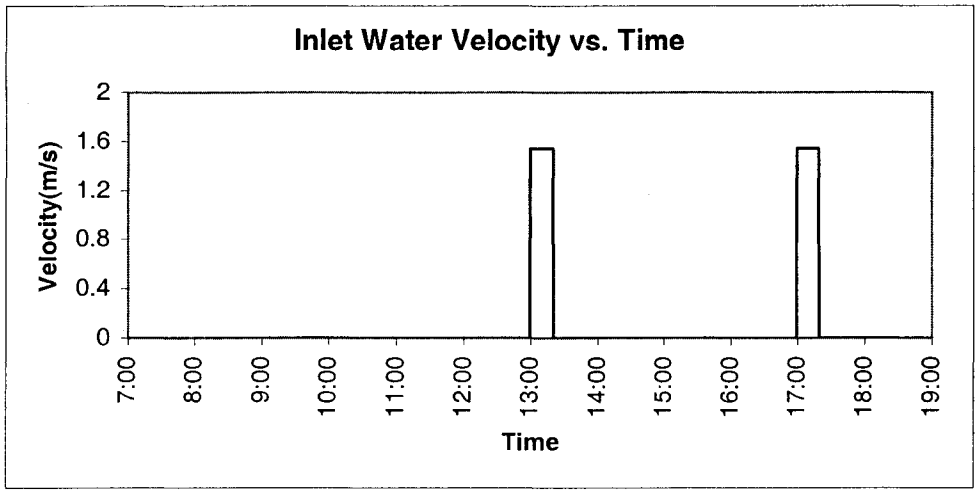

Figure 11: Profile of the inlet water velocity vs. time for hot water usage from 0700 to 1900

2.2.2. Forced convection closed loop solar water-heating system simulation

The numerical model for the forced convection solar water heater is a 3-D transient with total number of nodes as 205,000. The type of cell used was tetrahedral with a cell size approximately 5 mm for the collector and 20 for the reservoir. The 3-D model was made in a CAD program Solid Works and was meshed in the Star CD. The time step used for simulations was 15 seconds for all the cases and the simulations were performed for three different Reynolds numbers 500, 1000, and 1500.

The boundary condition for different sections of system is as follows:

1. Solar collector: The top surface of the solar collector was supplied with a boundary condition of heat flux with respect to time (figure 10) that will be acting as solar insolation [21].

2. Pipes, conical section, water reservoir and for bottom and side parts of the collector are supplied with adiabatic boundary condition.

3. Source momentum was supplied to simulate the effect of pump in the pipe section just below the water reservoir.

The numerical scheme used for both solar water heating systems are discussed briefly as follows:

1. A Boussinesq approximation was used to define density as a function of temperature. It was used to take into account the potential buoyancy effects in the reservoir that occurs due to mixing of hot water from collector and the cold water inside the tank. For natural convection case this is the main condition for setting up the flow inside the loop. Whereas in forced convection case its supplied to study the effect of mixed convection which may occur at low Reynolds number
2. PISO Algorithm was used for solving the transient problem.
3. AMG (Algebraic Multigrid) approach was used for solving matrix equations.
4. The numerical simulations were run in a transient mode for 12 hours of daytime i.e. from morning 0700am to evening 0700pm.

For more details about the numerical scheme please look in [20].

CHAPTER 3

RESULTS AND DISCUSSIONS

This chapter provides a detailed overview of the results of runs from simulations for natural convection open loop solar water heater model and forced convection closed loop solar water heater model. The numerical accuracy for the natural convection system was checked by satisfying the continuity equation at the top and bottom section of collector and reservoir respectively. The accuracy was found to be within 2.59 % for the collector and 0.32% for the water reservoir for the 4 hour of real time simulation data wherein the flow has been developed between the solar collector and water reservoir. The discussion shows the effect of the solar radiation on the temperature, velocity and mass flow rate of water in natural convection solar water heater as a function of time.

The discussion also shows velocity and temperature profiles and the effect of variation of Reynolds number on each of the above parameters for the forced circulation closed loop system. The parametric study was performed on this model for three different Reynolds number i.e. 1500, 1000 and 500 in the laminar flow regime. The separate simulation run was performed on closed loop system for 1500 Reynolds number in which the solar flux falling on the solar collector was considered to include the heat losses from the solar collector from top and sides. And the results of this run were compared with the runs with model that doesn't include any heat losses from the collector. The closed loop

system was also checked for numerical accuracy by checking the whether the system satisfies the continuity equation. The accuracy for closed loop system was found to be within 0.34 % for the collector. Finally the discussion explains the comparison between current study and the relevant literature.

3.0. Natural convection open loop solar water heating system

This section shows the results of the simulations at 2, 4, 6, 7.23, 10.5375 and 12 hour data in real time starting at 0700AM.

3.0.1. 2 hour real-time simulation data (0900AM)

Figures 12 and 13 show the velocity and temperature profile of the natural convection solar water heater. It can be observed that as the temperature of the water has rise from 305 K to 318.7 K in two hours of real time. As there is no momentum source in natural convection case, the water velocity slowly rises as the water gains heat from the solar collector. The gain in heat results in the density difference between the water at the top of the collector and the bottom of the reservoir because of which the water flows from the reservoir to the collector and vice versa which results in flow of water from the collector to the water reservoir.

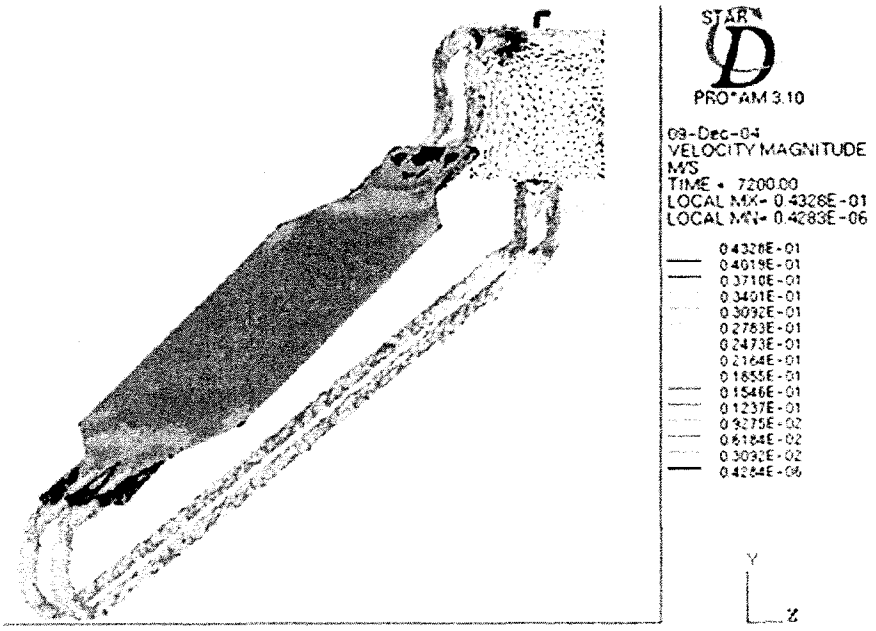

Figure 12: Velocity profile of complete system at 2 hours in real time

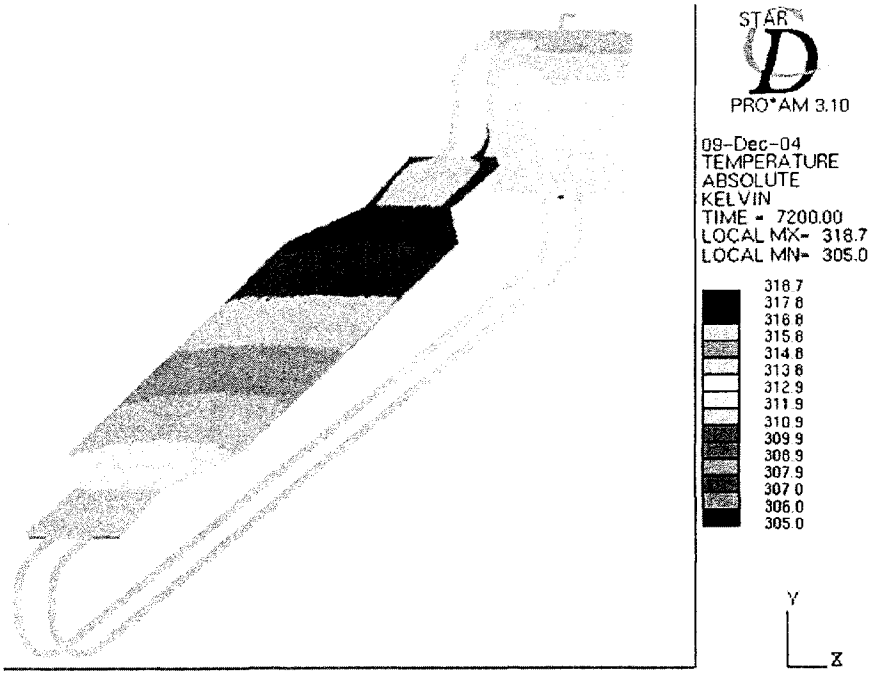

Figure 13: Temperature profile of complete system at 2 hours in real time

Figure 14 and 15 shows the temperature and velocity profile of the solar collector and the water reservoir. It can be clearly observed that as the water gains heat as it flows over the solar collector and flows towards the reservoir. As the water from the collector is at the higher temperature than the water reservoir, it moves upwards after entering the reservoir. Then after reaching the opposite end it starts moving down and mixes with the cold water in the reservoir resulting in the rise if water temperature inside the reservoir. This relatively hot water rises inside the reservoir and moves upwards and gets accumulated in the top layer of the reservoir as can be observed in the figure 15. And thus the water according to the temperature is stratified inside the reservoir with high temperature in the top and lower temperature at the bottom. Figure 15 also indicates the section of collector for figures 17, 18 and 19.

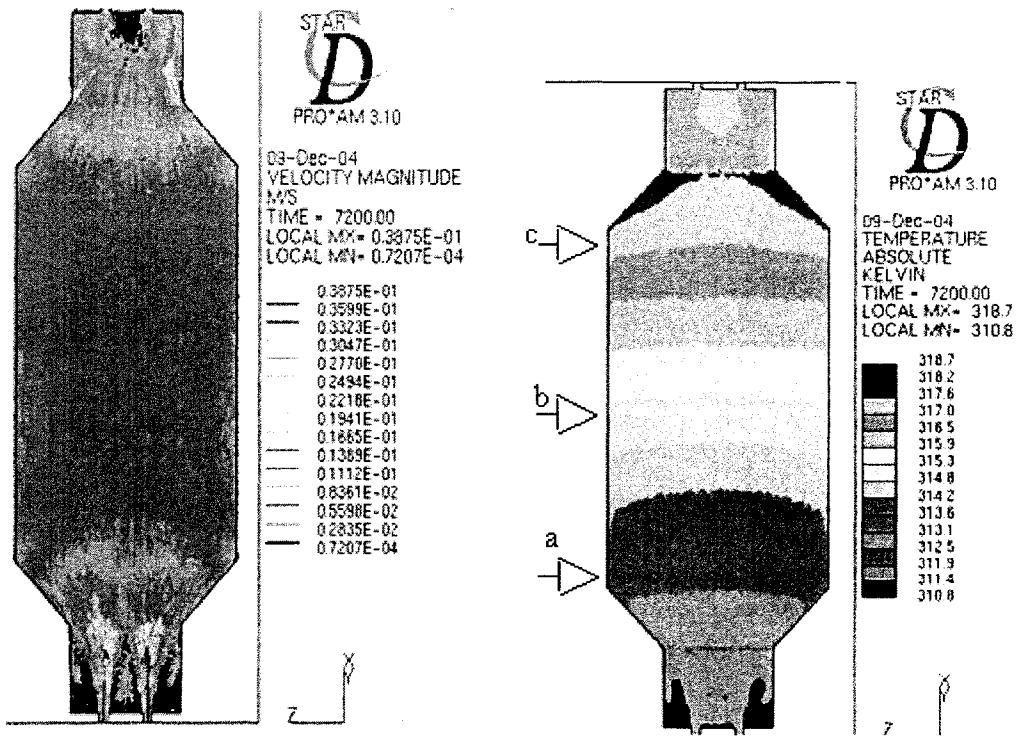

Figure 14: Velocity and temperature profiles of solar collector at 2 hours in real time

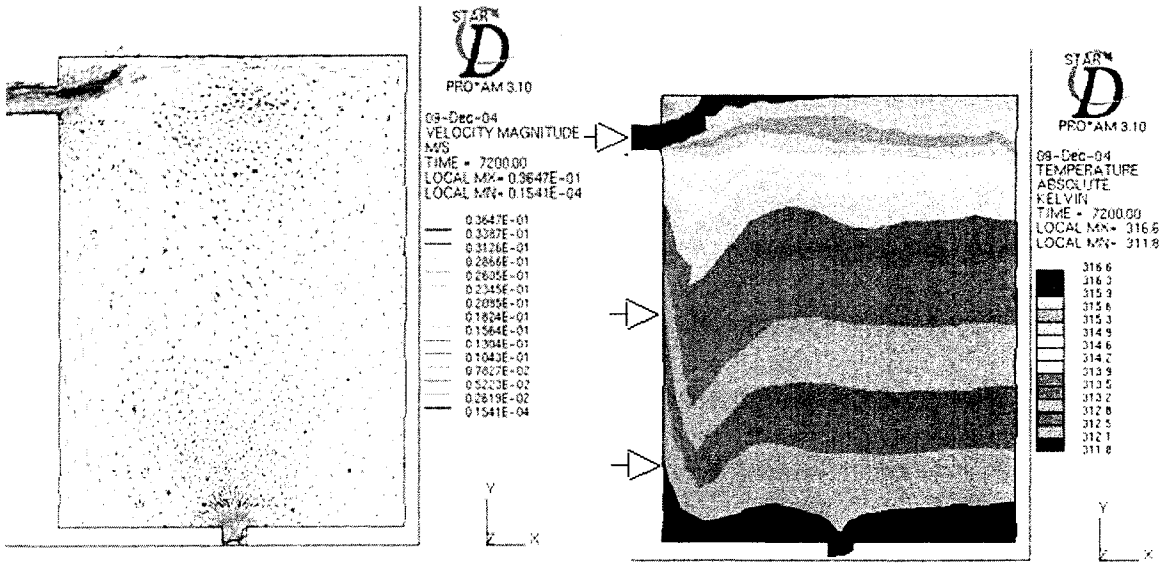

Figure 15: Velocity and temperature profiles of water reservoir at 2 hours in real time

Figure 16 and 17 shows the section of reservoir at which water enters the reservoir. It can be clearly seen that the water moves upwards and then to the opposite end inside the reservoir, it is then diverted in the different directions along the surface of the reservoir.

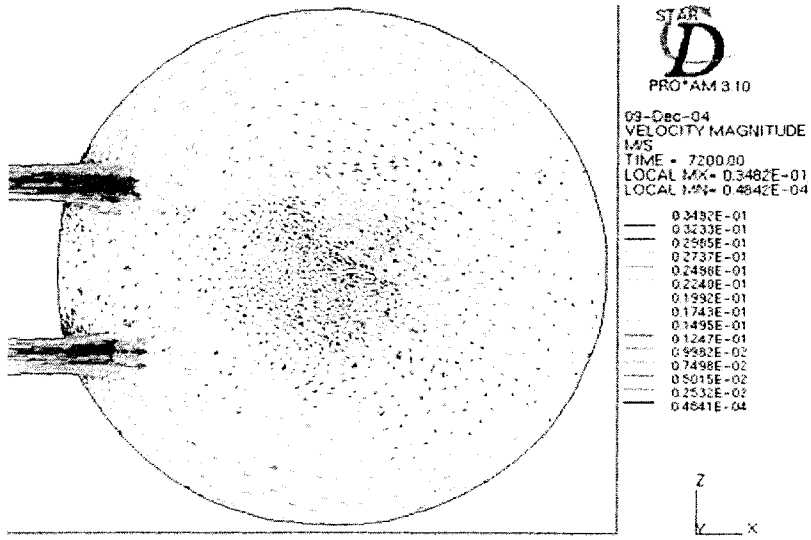

Figure 16: Velocity profile at the section normal to water reservoir and connecting pipe from collector at 2 hours in real time

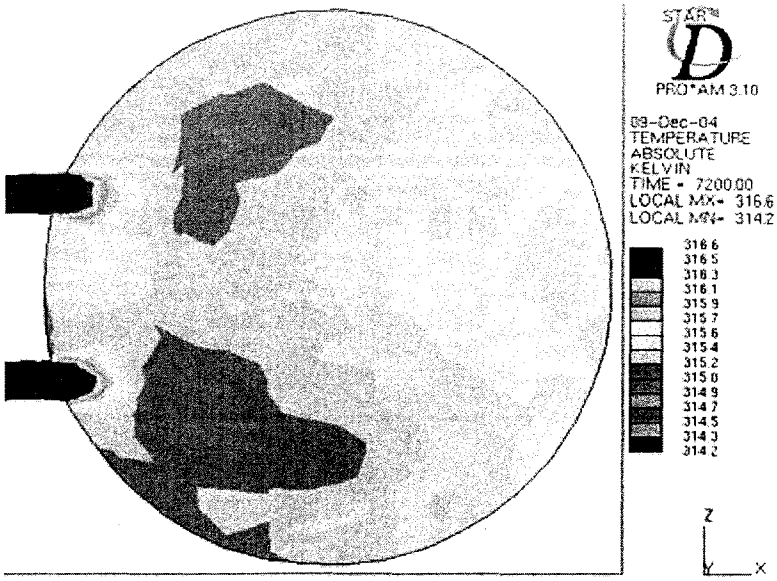

Figure 17: Temperature profile at the section normal to water reservoir and connecting pipe from collector at 2 hours in real time

Figure 18 shows the temperature profile at the middle of water reservoir. It can be observed that there are some localized hot zones that depict the zone from which the hot water rises towards the top of the reservoir. It also shows the mixing and heat convection from hot water to the relatively cold water at this section.

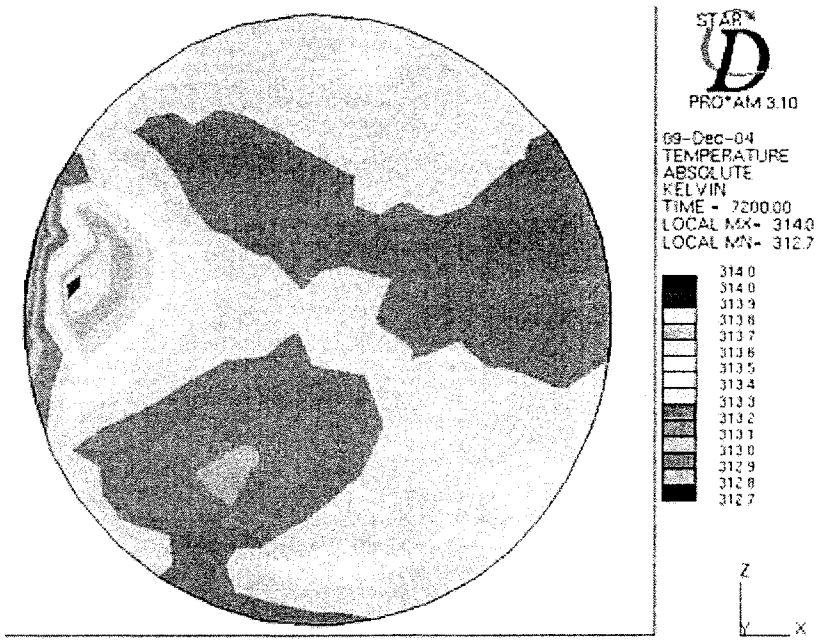

Figure 18: Temperature profile at the section normal to middle of water reservoir at 2 hours in real time

Figure 19 shows the temperature at section located at the bottom of the water reservoir. It can be observed that there are some localized hot zones here from which the heat is convected from the hot water to the cold water at this section. As the section is at the bottom the temperature difference at this section is relatively smaller to the other two sections which are at the middle and top of the reservoir.

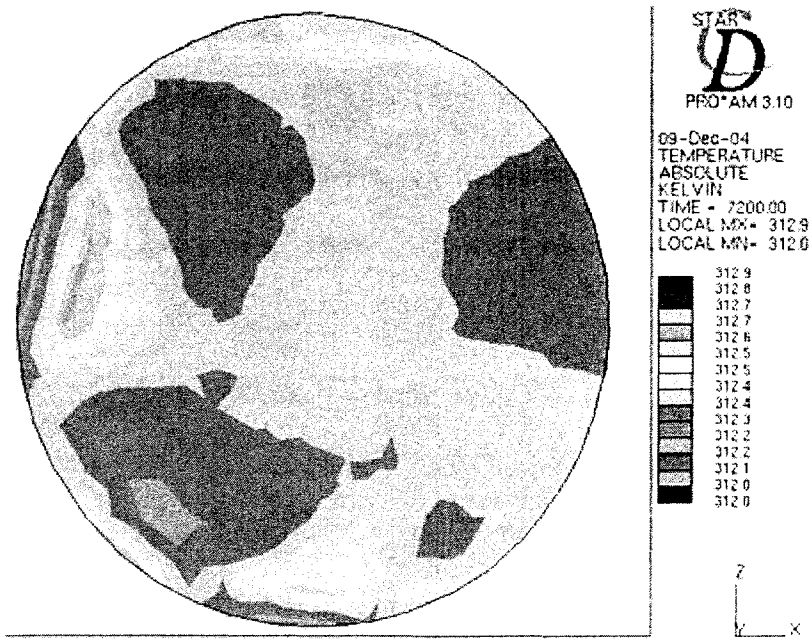

Figure 19: Temperature profile at the section normal to bottom of water reservoir at 2 hours in real time

Figure 20 and 21 shows the velocity and temperature profile of the conical section at the intersection between pipe and solar collector where the cold water enters the solar collector. It can be observed that as the water enters the conical section it spreads and moves towards the collector. There are some localized flow zones where there is some eddy formation. The temperature of the water rises as it leaves the conical section and comes in contact with the solar collector.

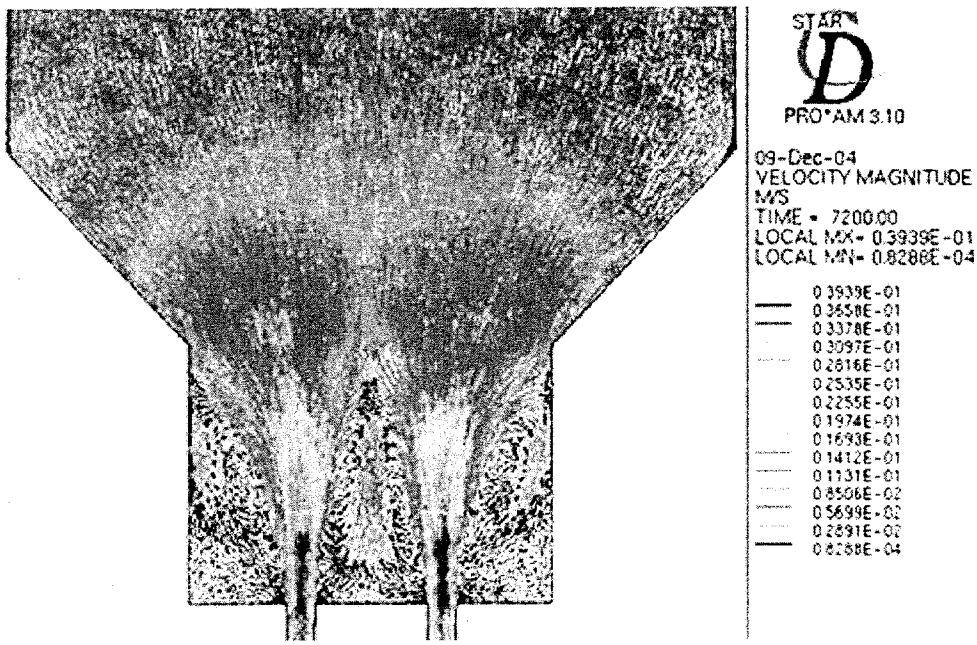

Figure 20: Velocity profile of the conical section at the bottom of collector at 2 hours in real time

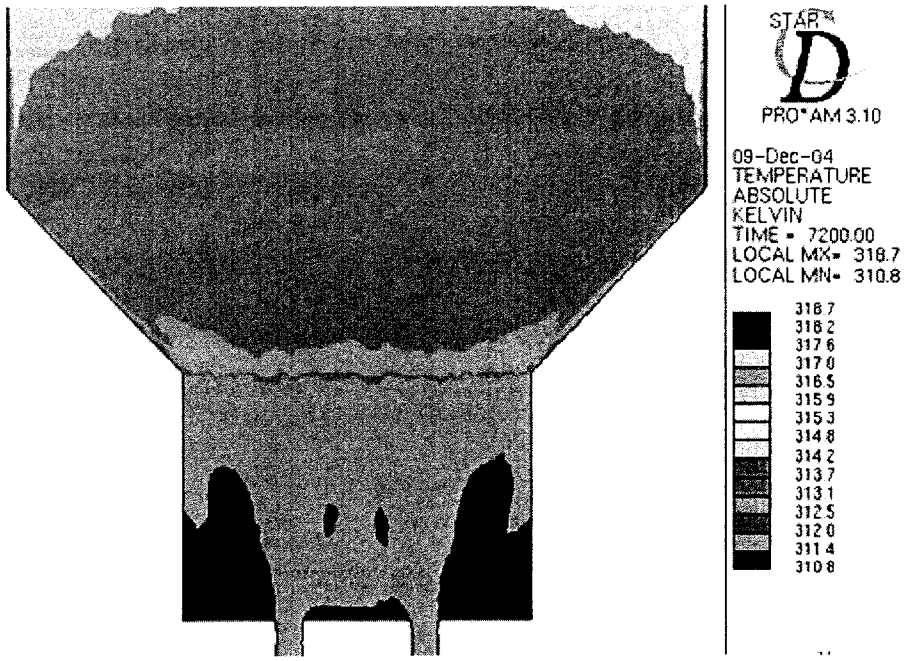

Figure 21: Temperature profile of the conical section at the bottom of collector at 2 hours in real time

Figures 22 and 23 shows the velocity and temperature profile of the conical section at the intersection between pipe and solar collector where the hot water leaves the solar collector. It can be observed that there is a single localized flow zone. There is stagnation of water inside this zone and water flows around it to enter the pipes connected to the conical section.

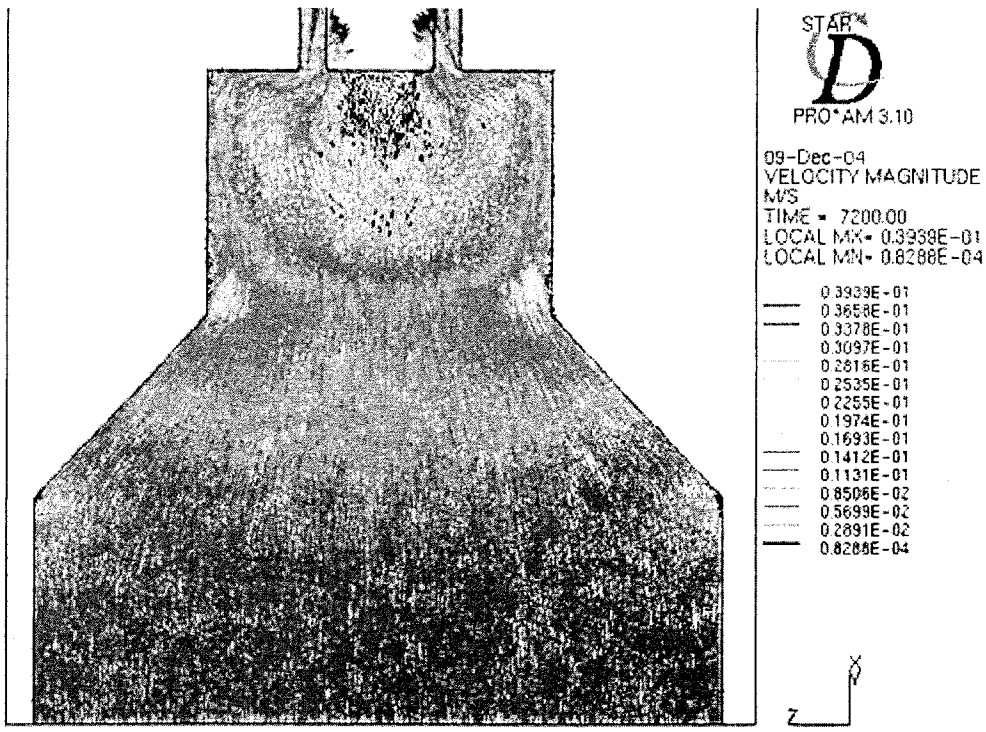

Figure 22: Velocity profile of the conical section at the top of collector at 2 hours in real time

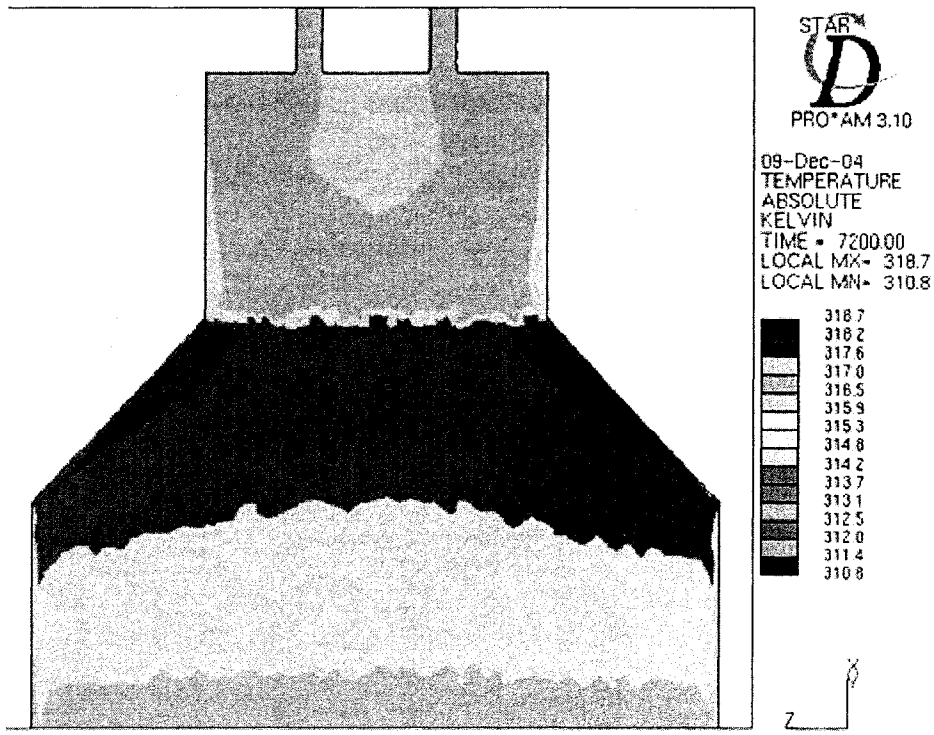

Figure 23: Temperature profile of the conical section at the bottom of collector at 2 hours in real time

Figure 24 shows the temperature profile inside the solar collector at the sections a, b and c shown in figure 14. All of these sections are located at the section where there is no change in cross section area across the collector. It can be observed that as the water gains heat as it moves along the length of the collector.

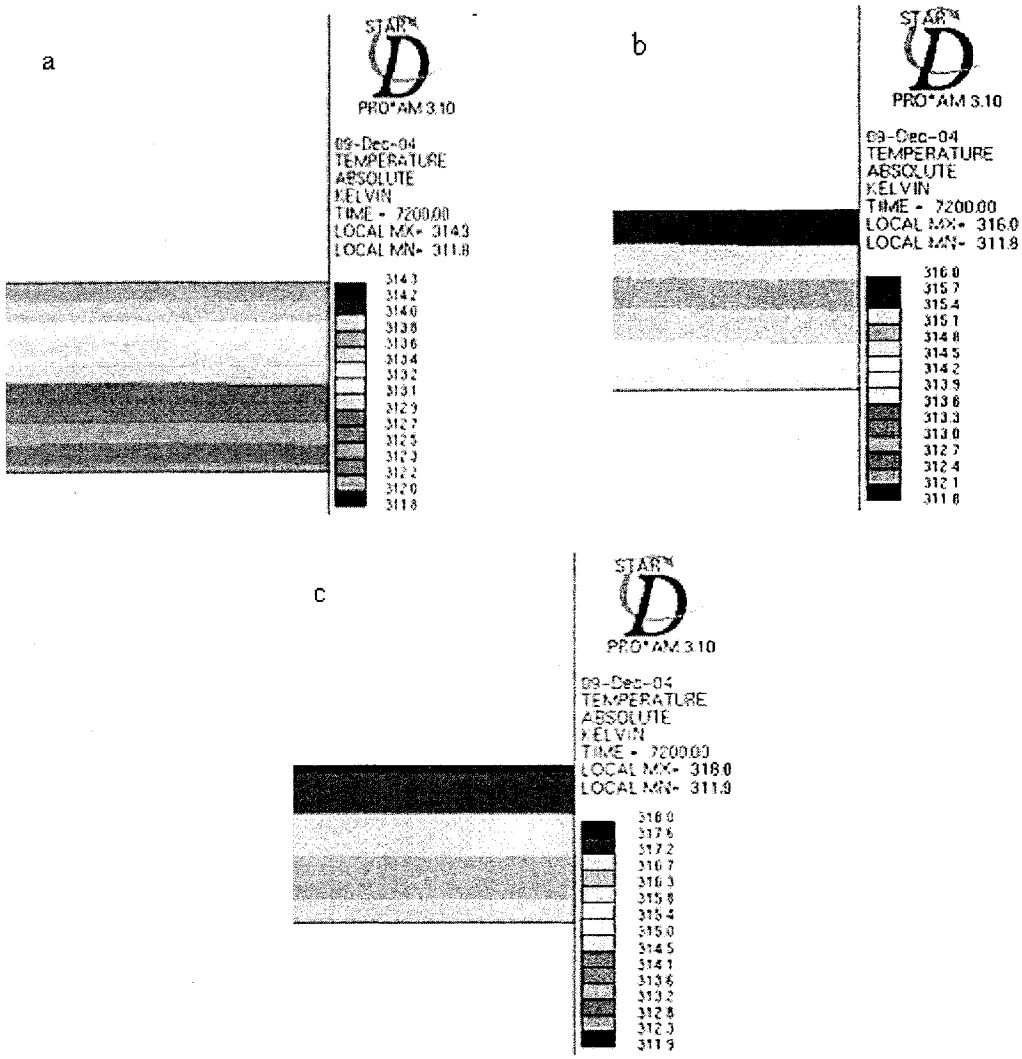

Figure 24: Temperature profile of the collector at various sections (a- bottom, b-middle and c-top section) at 2 hours in real time

3.0.2. 4 hour real-time simulation data (01100AM)

Figures 25 and 26 show the velocity and temperature profile after 4 hour of real time simulation. It can be observed that as the daytime increases there is increase in velocity as well as in the temperature of the solar collector.

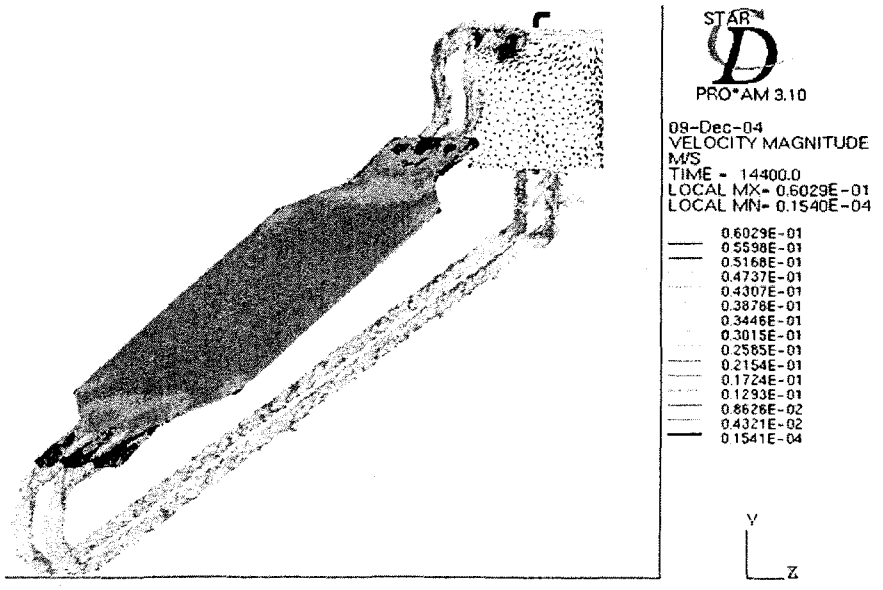

Figure 25: Velocity profile of complete system at 4 hours in real time

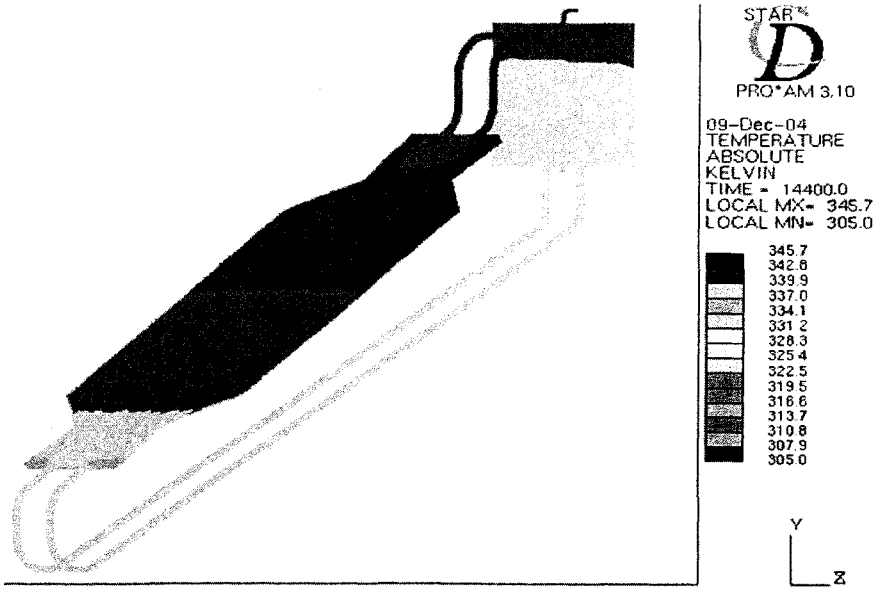

Figure 26: Temperature profile of complete system at 4 hours in real time

From figure 27 it can be observed that there is not only increase in temperature of water inside the collector but also in the temperature difference across the collector which

shows the increase in the heat gained by water due to increase in the solar heat flux acting on the collector. There is also increase in the flow velocity inside the collector.

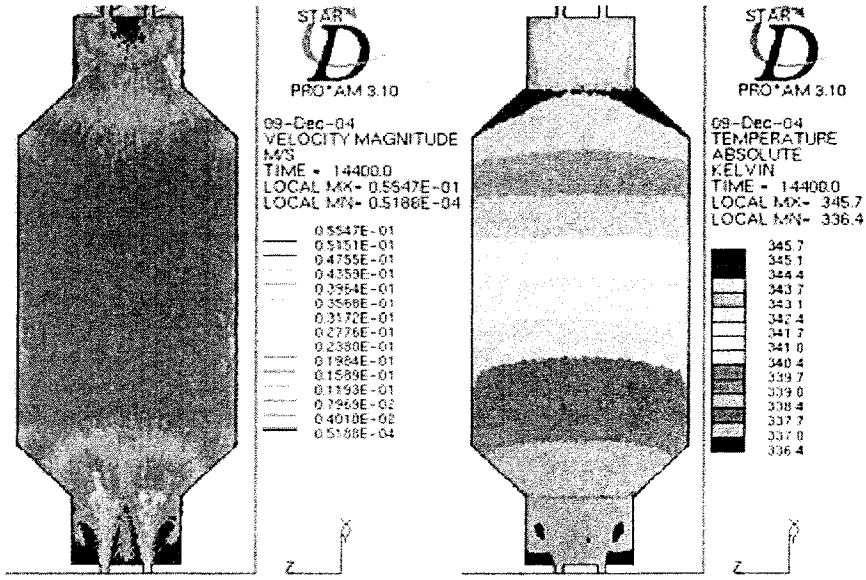

Figure 27: Velocity and temperature profiles of solar collector at 4 hours in real time

From figures 28 it can be observed that there is significant rise in temperature of water inside the reservoir. The flow velocity inside the reservoir has also increased resulting in proper mixing and stratification inside the reservoir.

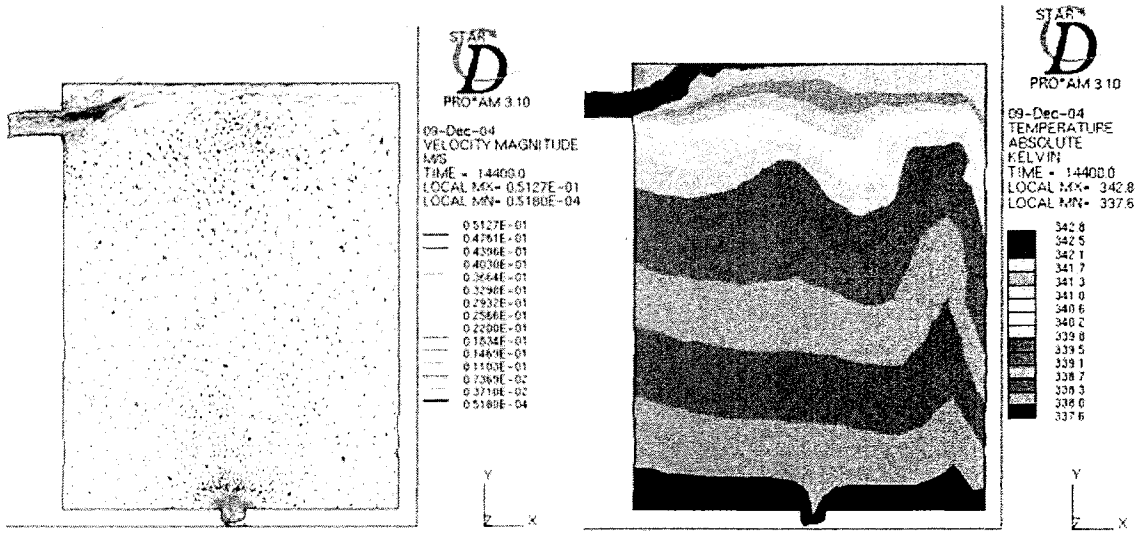

Figure 28: Velocity and temperature profiles of water reservoir at 4 hours in real time

3.0.3. 6 hour real-time simulation data (0100PM)

Figures 29 and 30 show the velocity and temperature profile at 1:00 pm real-time. It can be observed that there is hot water coming out of the solar water heater from the outlet due to the imposed inlet condition at the inlet. The mass flow rate of the water from outlet is relatively higher than the operating flow rate inside the solar water heater. In the temperature profile it can be clearly observed that the temperature of cold water entering the water reservoir results in localized stratification at the bottom of the tank from the water at higher temperature inside the reservoir and the incoming water at relatively lower temperature. It can also be observed that the temperature of water is highest on the top of the water reservoir from where the hot water flows out for domestic usage.

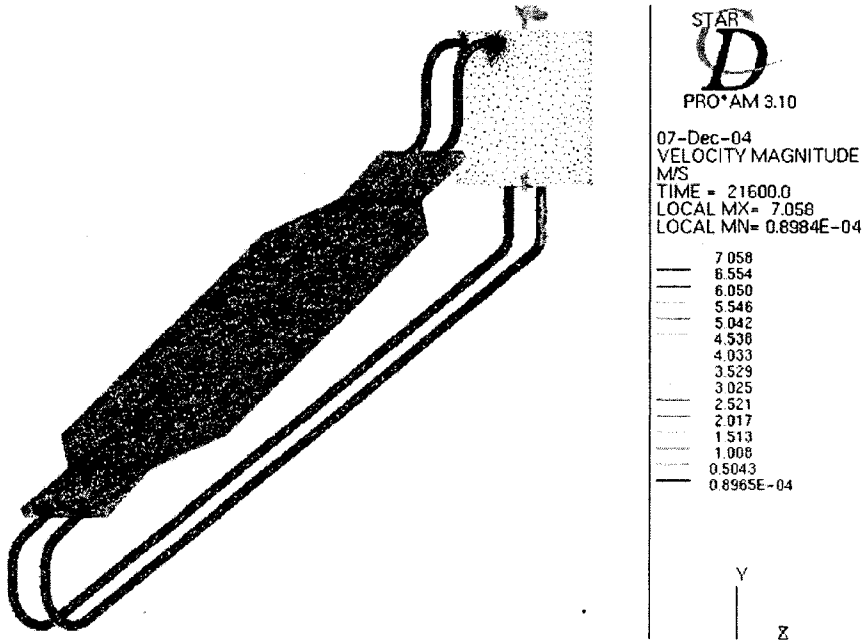

Figure 29: Velocity profile of complete system at 6 hours in real time

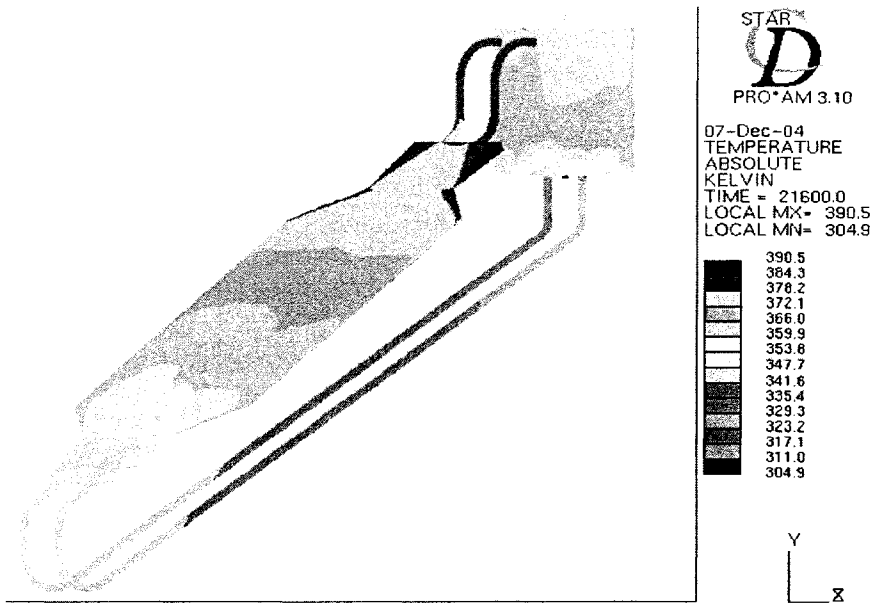

Figure 30: Temperature profile of complete system at 6 hours in real time

Figure 31 shows the velocity and temperature profiles of the solar collector at 6 hours in real time. It can be observed that the collector reaches the maximum temperature at the 6 hours as there is maximum solar heat flux acting on the collector surface.

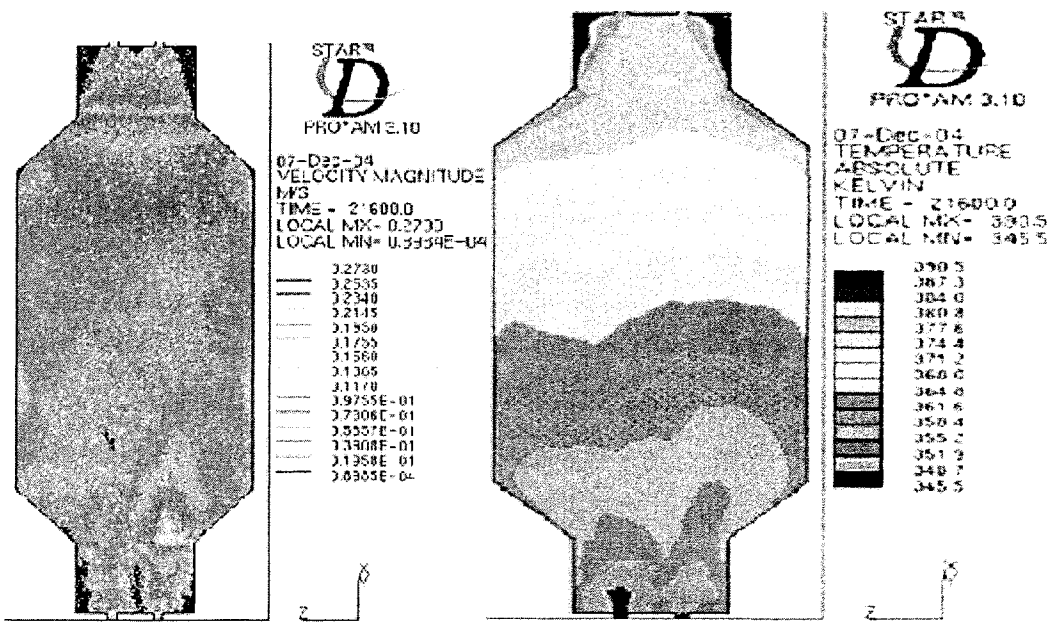

Figure 31: Velocity and temperature profiles of solar collector at 6 hours in real time

Figure 32 shows the velocity and temperature profile in the section of inlet and outlet pipe of the water reservoir. From the velocity profile it can be observed that as the capacity of tank is large, the effect of the inlet flow rate is very small on the flow inside the tank which results in mixing and stratification inside the tank. From temperature profile it can be observed that though at the bottom of the reservoir there is some stratification of temperature, top of the reservoir still contains the water at higher temperature. The top left part of the temperature profile (section 'a' in figure 32) shows the higher temperature as compared to the top right part because of the effect of entering

hot water from collector on the top left part and outgoing hot water from top of the reservoir.

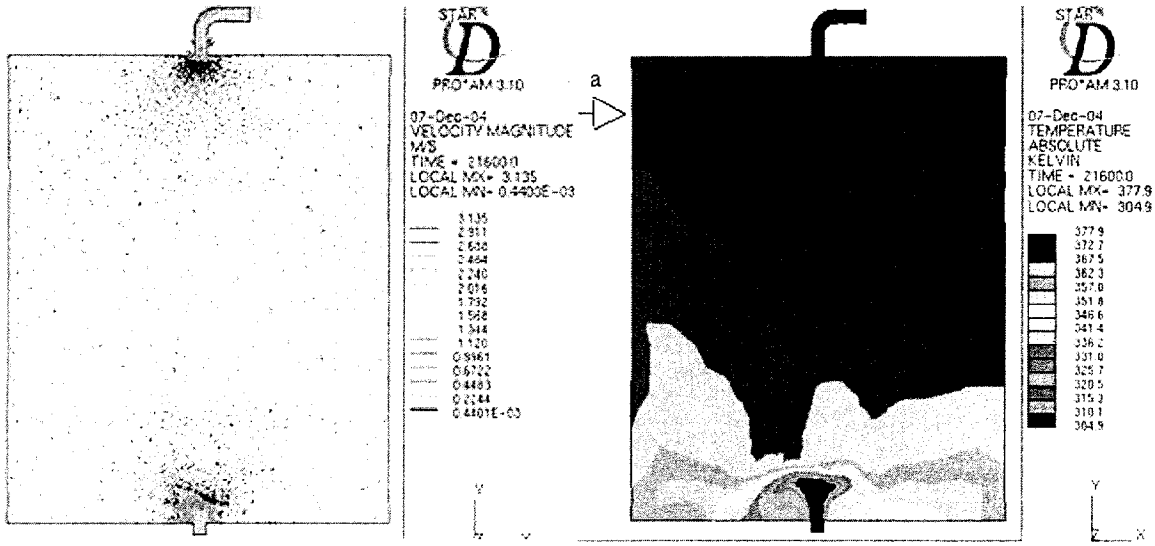

Figure 32: Velocity and temperature profiles of water reservoir at 6 hours in real time

3.0.4. 7.23 hour real-time simulation data (0213PM)

Figures 33 and 34 show the velocity and temperature profile at 7.23 hour real time data. It can be observed that after the water has been tapped at the interval 1 there is reduction in the temperature in the whole system. Due to which the velocity and eventually the flow rate has been reduced. But the as there is some density difference still there between the top of collector and bottom of the reservoir to enable the flow between the collector and reservoir.

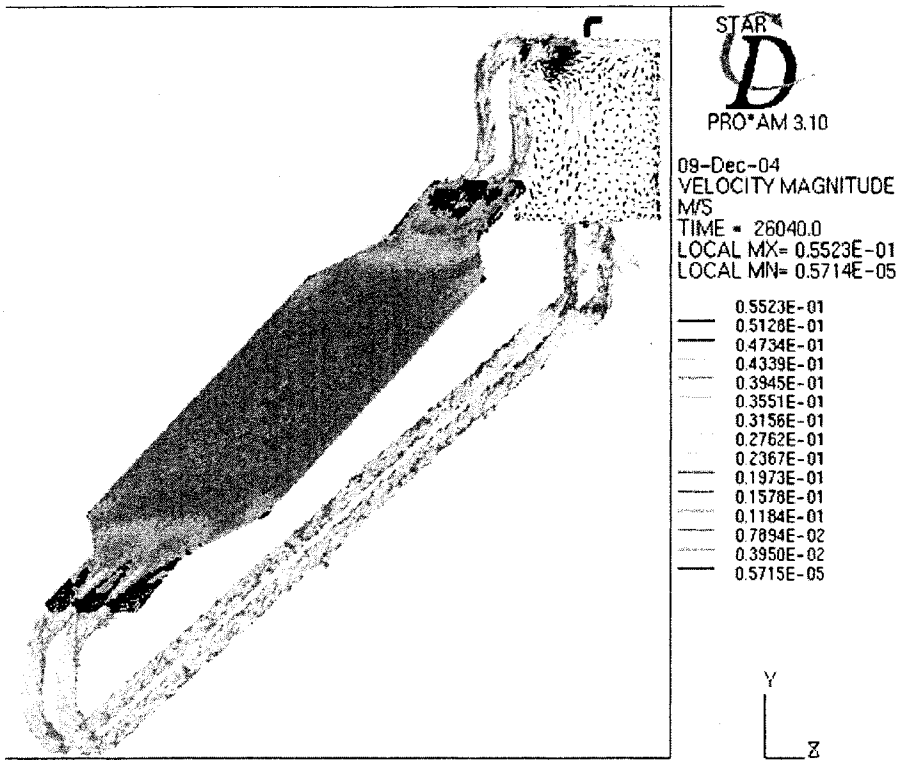

Figure 33: Velocity profile of complete system at 7.23 hours in real time

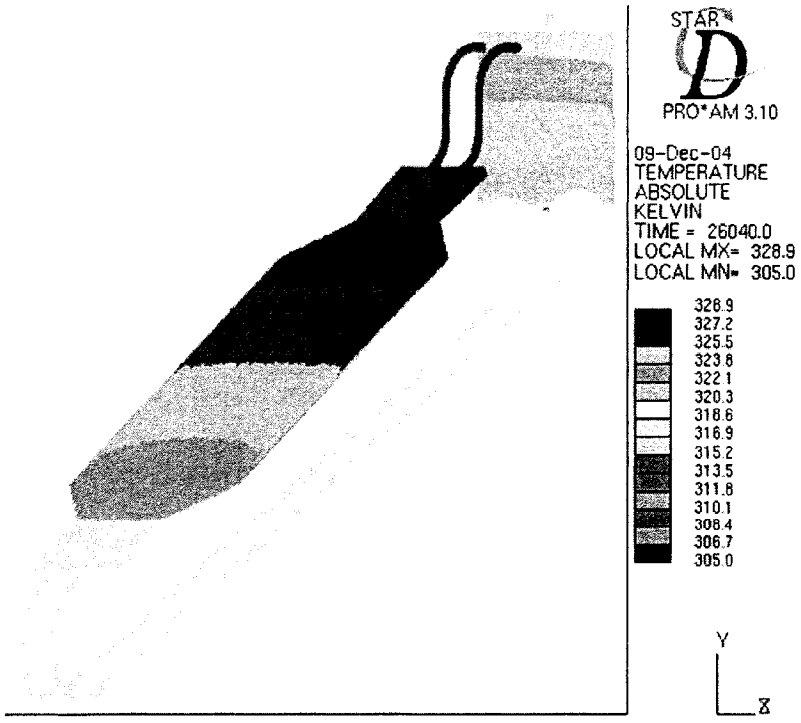

Figure 34: Temperature profile of complete system at 7.23 hours in real time

Figure 35 shows the temperature and velocity profile of collector at 7.23 hrs real time. It can be observed that the there is reduction in entry and exit temperature as compared to the 6 hours real time simulation data which clearly shows the effect of the water usage on the solar water heater. Fig 36 shows the velocity and temperature profile inside the reservoir for the same time. From velocity profile, it can be observed that there is a closed loop of flow inside the reservoir, which results in proper mixing and stratification of hot and relatively cold water inside the reservoir.

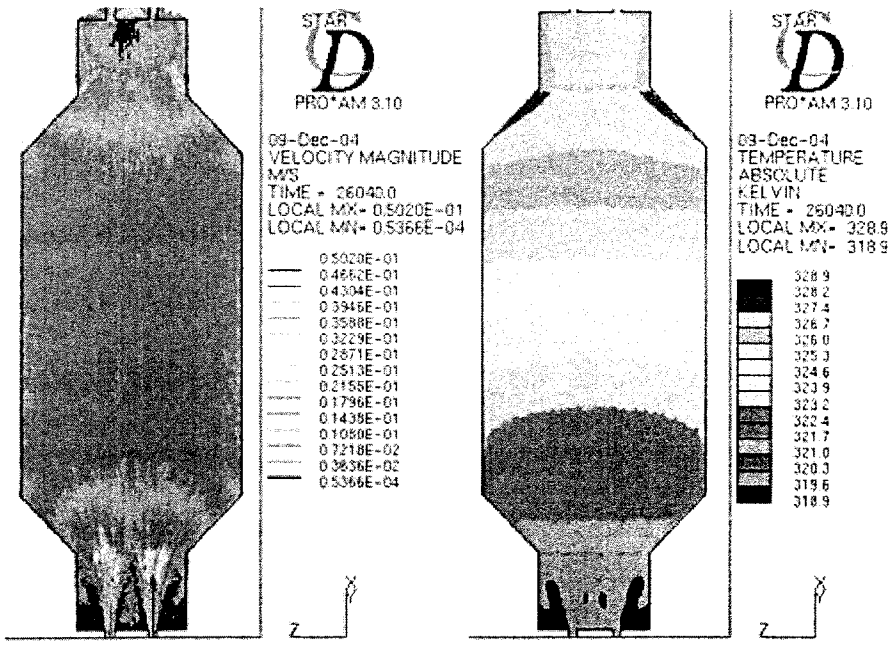

Figure 35: Velocity and temperature profiles of solar collector at 7.23 hours in real time

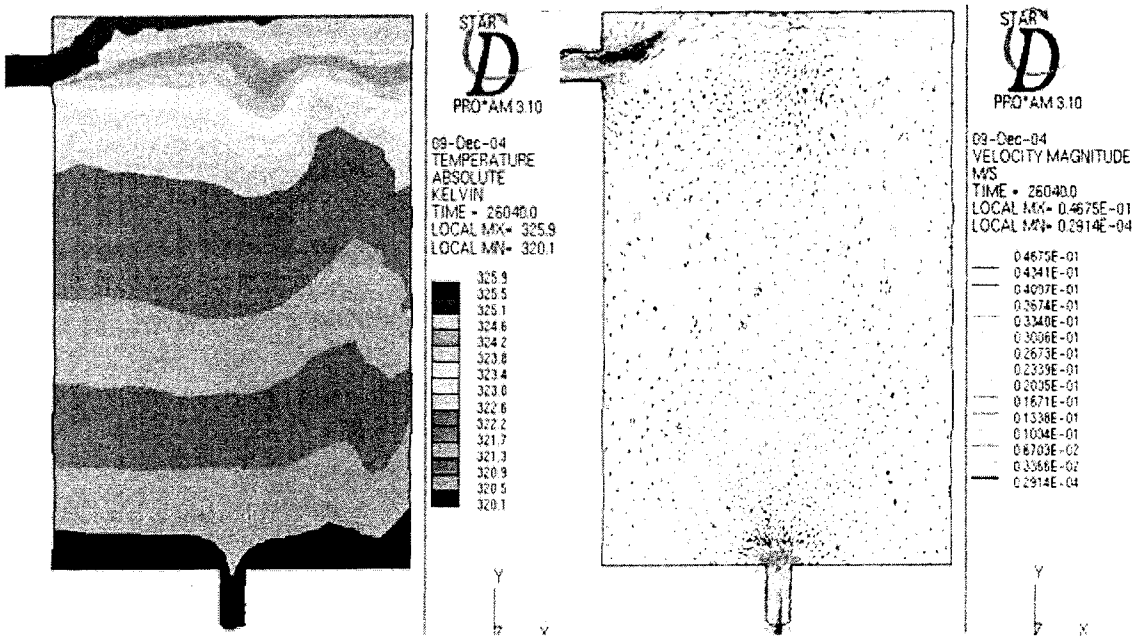

Figure 36: Velocity and temperature profiles of water reservoir at 7.23 hours in real time

3.0.5. 10.5375 hour real-time simulation data (0532PM)

Figures 37 and 38 show the velocity and temperature profile after the 10.5375 hours in real time that is after the second interval of water usage. It can be observed that velocity and hence the flow rate inside the system has reduced and also the maximum temperature of the system. It is due to water usage at the second interval and also as the heat flux at the solar collector is reducing gradually according to the real time.

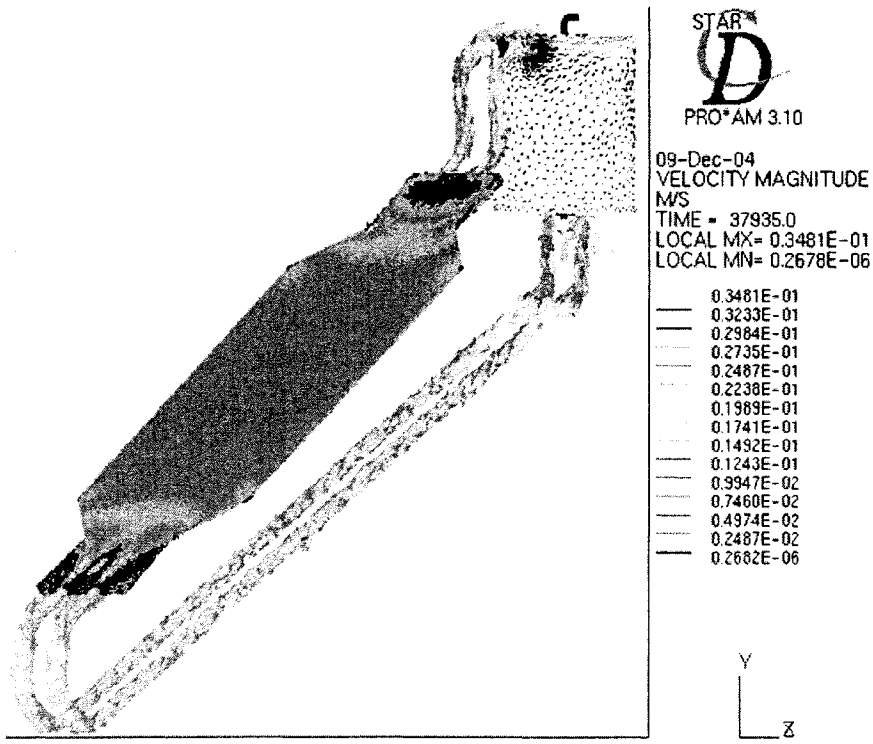

Figure 37: Velocity profile of complete system at 10.5375 hours in real time

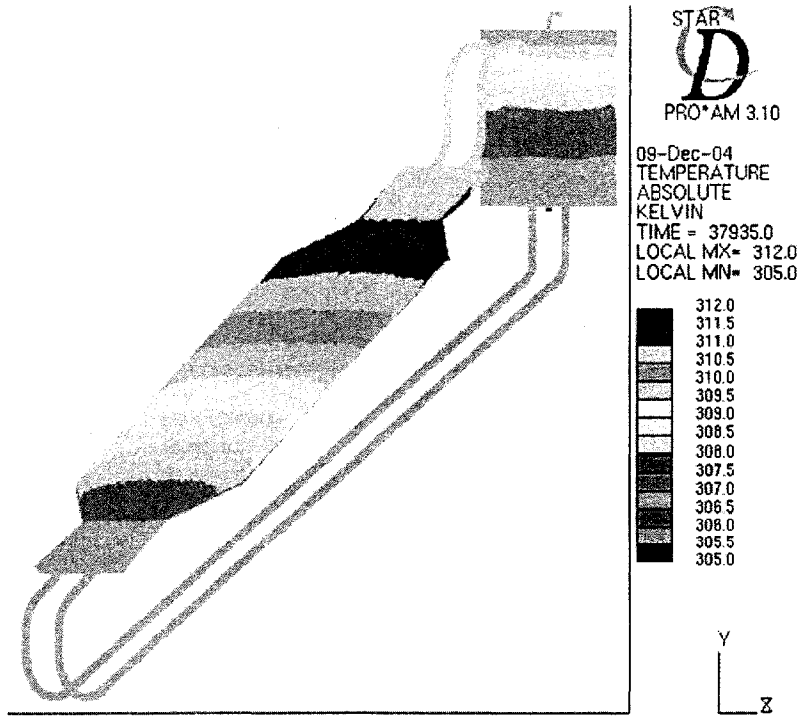

Figure 38: Temperature profile of complete system at 10.5375 hours in real time

Figure 39 shows the velocity and temperature profile inside the collector. It can be clearly observed that as the temperature rise in the collector has reduced with the reduced heat flux on the solar collector. From figure 40 it can be observed that with the reduction in velocity and hence flow rate the bottom part of the reservoir is at the constant temperature. It is because with the reduction in flow rate affects the mixing and stratification inside the tank.

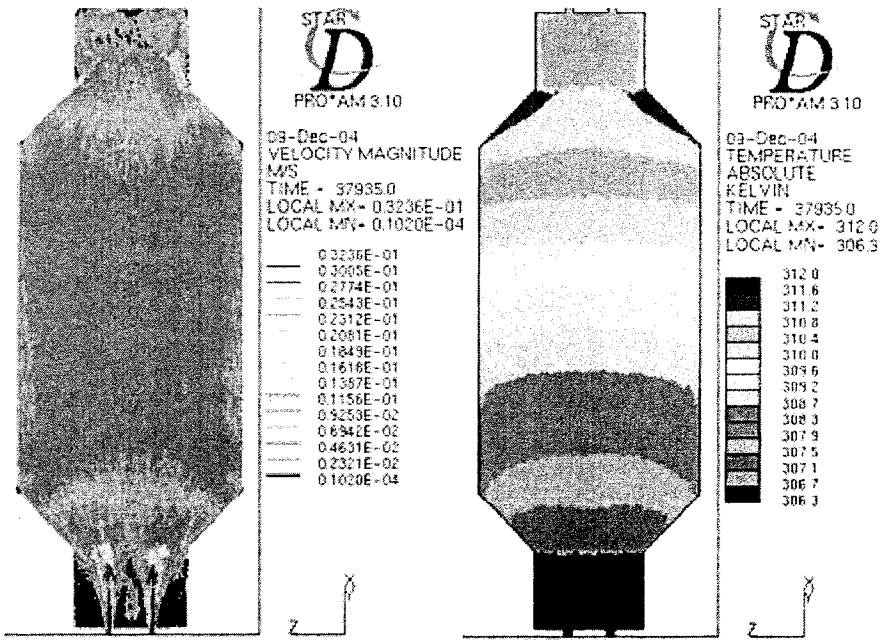

Figure 39: Velocity and temperature profiles of solar collector at 10.5375 hours in real time

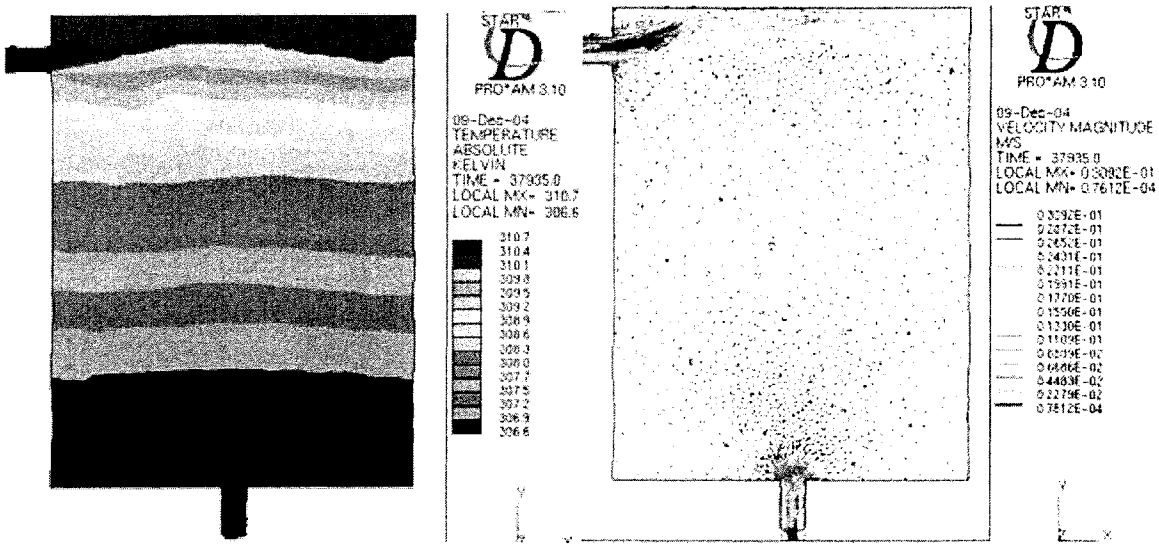

Figure 40: Velocity and temperature profiles of water reservoir at 2 hours in real time

3.0.6. 12 hour real-time simulation data (0700PM)

Figures 41 and 42 show the velocity and temperature profile in the solar water heater at the end of 12 hour real time simulation. It can be observed that there is increase in flow rate and maximum temperature in the system as compared to the 10.5375 hours real time simulation data. This is due to the fact that water was gaining heat from the solar collector for rest of the day. It can be observed that at the end of the day there is increase in 8.6 Deg C in temperature rise from the base temperature.

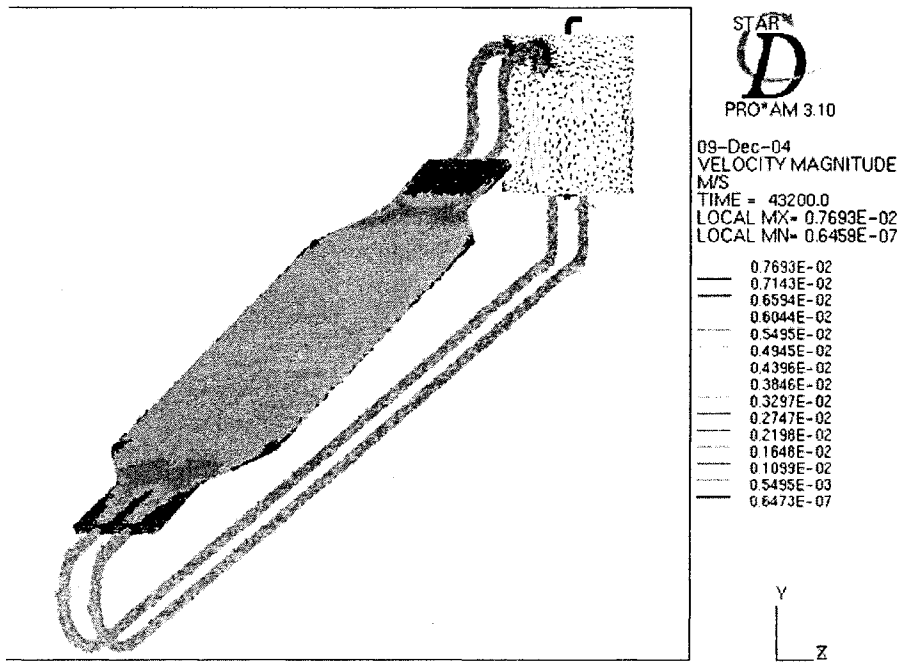

Figure 41: Velocity profile of complete system at 12 hours in real time

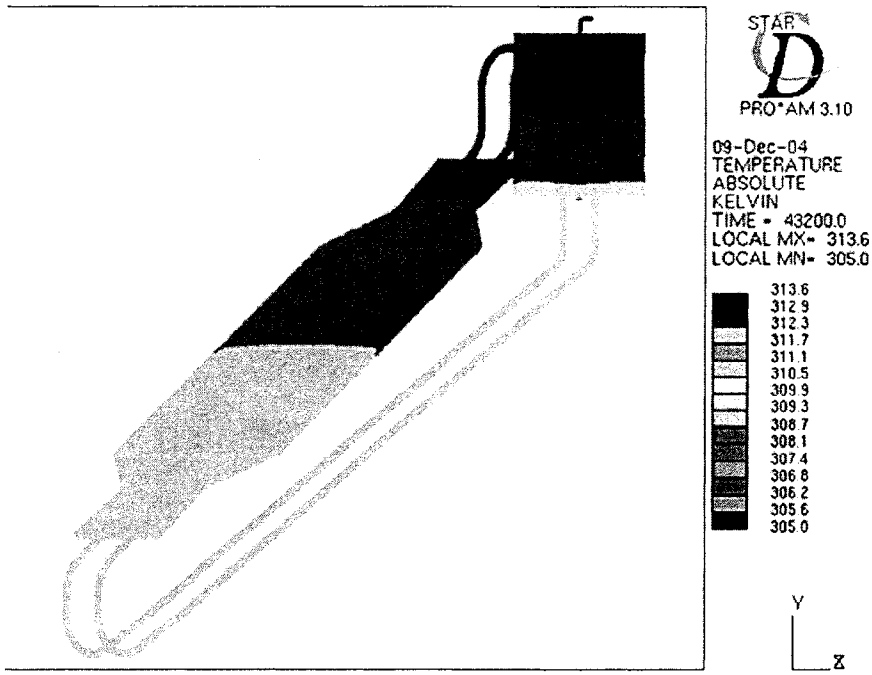

Figure 42: Temperature profile of complete system at 12 hours in real time

From figure 43 it can be observed that the temperature rise across the collector is reduced significantly. The flow rate is also reducing across the collector. But as the water is still flowing from the collector to the reservoir in the normal direction it can be observed that till the 12 hour real time there is no effect of hydrodynamic instability inside the system. This hydrodynamic instability occurs during the night when the nocturnal radiation is falling on the collector which results in the reverse flow of water from the reservoir to the collector. But as for our case, we are running during the day time from 0700am to 1900 am the possibilities of the hydrodynamic instability is eliminated.

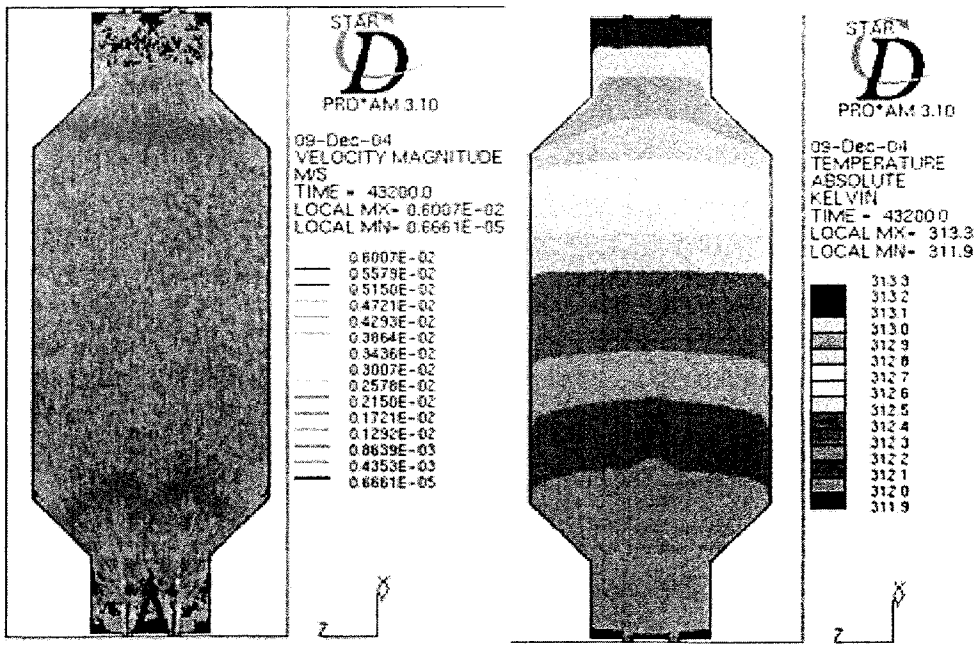

Figure 43: Velocity and temperature profiles of solar collector at 12 hours in real time

From figure 44 it can be observed that as the temperature of incoming water from the collector is low as compared to the water inside the reservoir, the water moves in

downward direction after entering the reservoir. And then after interacting with the hot water inside the reservoir it rises further and mixes with it. It can be also observed from temperature of water inside the reservoir is high as compared to the water entering from the collector.

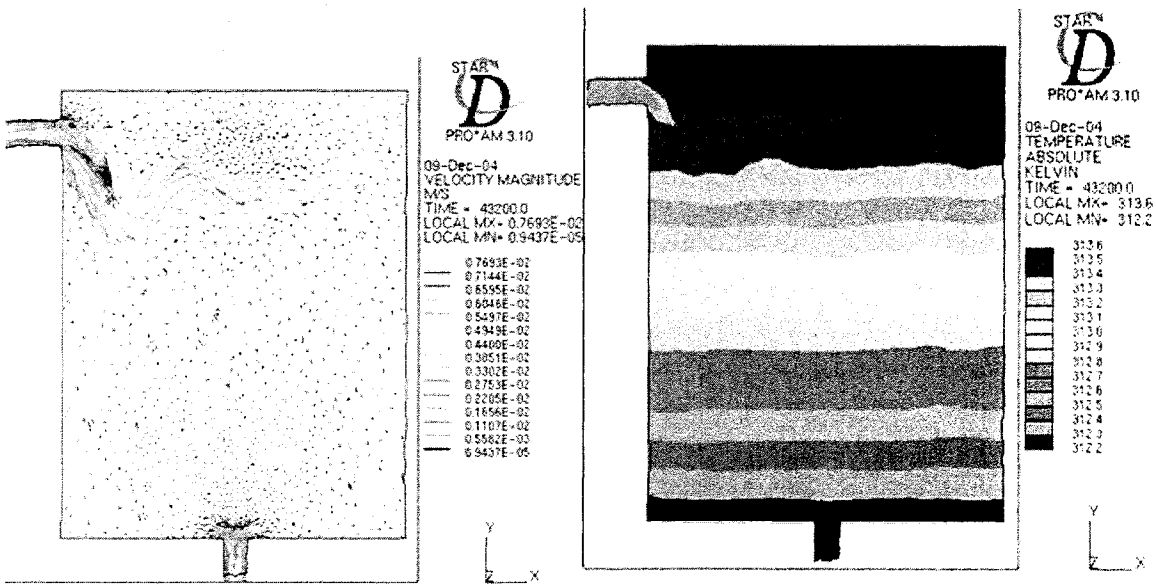

Figure 44: Velocity and temperature profiles of water reservoir at 12 hours in real time

Figure 45 shows the mass flow rate, maximum water temperature and there variation with respect to time at the section 'c' (figure 14) of collector. It also shows the effect of the water usage schedule on the flow rate and water temperature on the top of the solar collector. It can be observed from the figure that as the day time progresses there is increase in flow rate as well as the water temperature in collector which reaches to the maximum when there is maximum solar flux acting on the collector. From literature its been found that though the trend in which the water temperature and flow rate behaves during the day time and also during the water usage time are similar to the experimental results [22] but as the heat losses from the system are not taken into

account, our system reaches the peak temperature and maximum flow rate at the time of maximum solar heat flux acting on the solar collector. After the water usage in first interval, it can be observed that there is reduction in water temperature and flow rate. In fact the water temperature and flow rate rises between the first and second interval similar to the time from start time and first interval but as we didn't had any intermediate data from 0213 PM till 0534 PM due to the programming problem on the software; the behavior seems to be different from the behavior shown in figure 45. Finally after the second interval of water usage the system again gains the heat from the collector and at the end of the day temperature of water is higher that the initial temperature by 9 deg C.

From figure 45 it can be observed that the maximum temperature obtained for our case is over predicted due to the fact that in order to simplify the calculations the heat losses from the solar water heating systems were not taken into consideration which would have added an addition effort to simulate the model. But if the heat losses would have been accounted then the system may have predicted a realistic picture of performance of the model.

It was found [22] by applying and then modifying the heat loss coefficients as function of ambient and collector temperature [17] to the model can significantly improve the solution to the more realistic one i.e. the one which can be expected to validated with the experimental results. It's been found that [5] the heat loss coefficients are very sensitive to the location and time which makes the simulations difficult and also to validate with the experimental results. As there is no experimental data available for the system we have proposed, there is a very less room for validating the results of the simulations. If we assume the heat losses to be 20 % then the maximum water outlet

temperature from collectors validate with the experimental work presented in the literature [8], but this results were for the flat plate and tube type of collectors whose thermal performance would be different from collector what has been proposed.

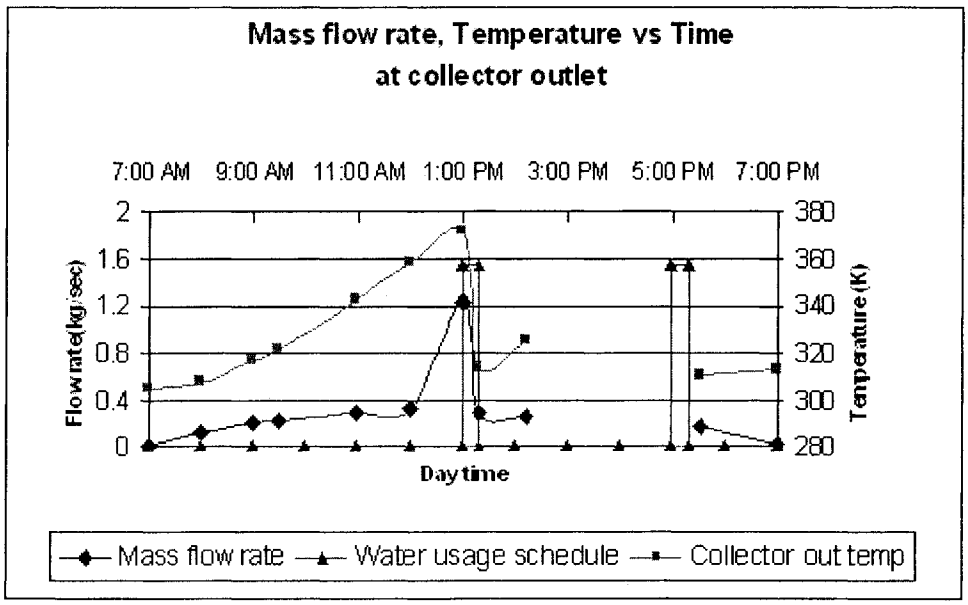

Figure 45: Collector outlet behavior for the natural convection open loop solar water heating system

Figure 46 shows the thermal behavior of the reservoir with respect to time. The behavior of mean reservoir temperature is similar to the collector outlet temperature except at 0100 PM when the temperature in the lower part of the reservoir is reduced due to the lower temperature of inlet water. At this time i.e. 0100 PM though the temperature in top portion of reservoir is high but due to reduction in the temperature in lower portions the mean reservoir temperature reduces.

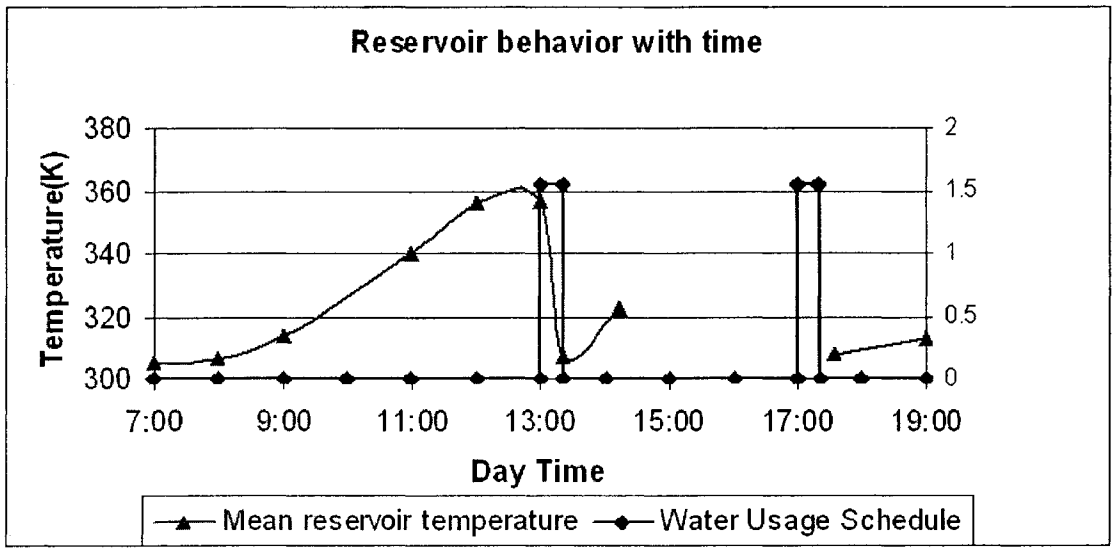

Figure 46: Reservoir mean temperature for the natural convection open loop solar water heating system

3.1. Forced convection closed loop system solar water heating system

This section shows the results of the simulations at 1.5 and 12.22 hours in real time starting at 0700AM. Due to the programming problem the simulations were run for 12.22 hours instead of the 12 hours in real time. The closed loop system as explained in previous chapter has two main components namely solar collector and the reservoir connected with the piping system. The real time simulation was performed for 12.22 hours of the daytime from 0700AM to 19:13PM. But for the time from 12 hours to 12.22 hours in real time the heat flux acting on the collector was zero watts/sq. m.

3.1.1. Simulation data at 1500 Reynolds Number

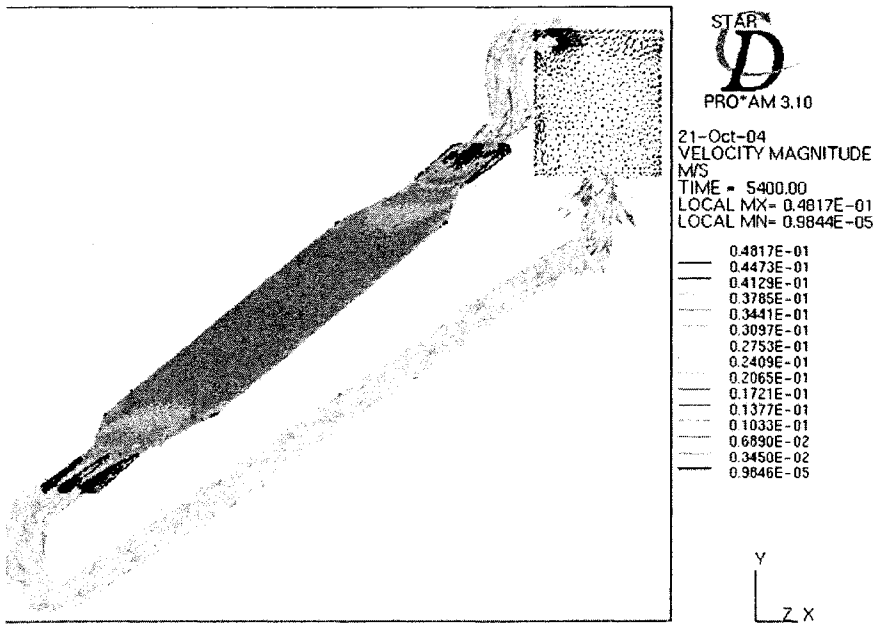

Figure 47: Velocity profile of closed loop solar water heater after 1.5 hours in real time

From figure 47 it is observed that when the water enters from the conical section to the solar collector there is a reduction in velocity due to the fact of change in the cross-sectional area of the solar collector. And the water gains the heat from the solar collector and thereby rises in the collector due to the momentum as well as due to the density difference between collector and reservoir. While the water enters the reservoir after getting heated in collector there is mixing between the hot water that is entering and the relatively cold water that is already present in the reservoir. This mixing eventually results in the stratification inside the reservoir that can be clearly observed in figure 48.

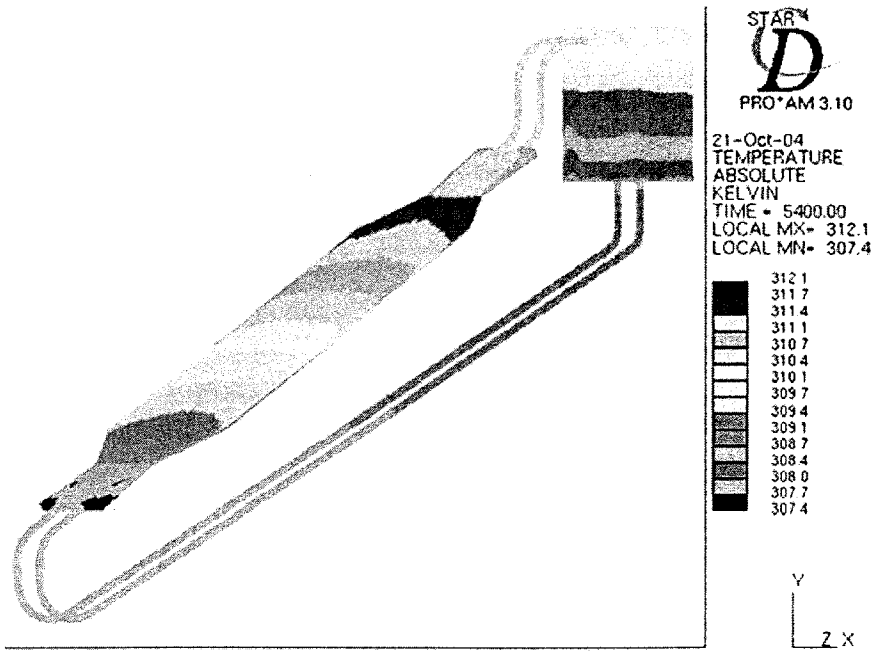

Figure 48: Temperature profile of closed loop solar water heater after 1.5 hours in real time

Figure 49 shows the velocity and temperature profile in the solar collector. It can be observed that as the water flows across the solar collector there is continuous rise in the temperature of water. The highest temperature in the system as well as solar collector is observed to be at the top portion of the solar collector.

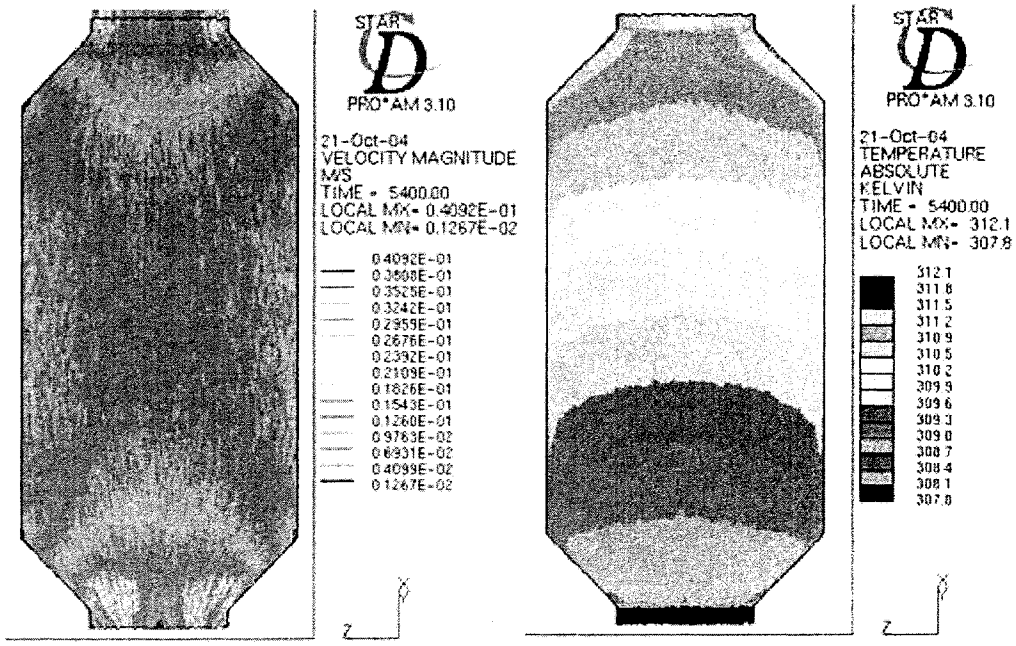

Figure 49: Velocity and temperature profile in solar collector after 1.5 hours in real time

Figures 50 show the velocity and temperature profile of the water reservoir and the partial sections of pipe that connects it to the solar collector. The pattern in which the hot water coming from the collector mixes and flows inside the water reservoir can be clearly observed. The hot water from solar collector enters the water reservoir and rises to the top of it and then moves to the opposite end of the reservoir from where it starts moving down and mixing with the relatively cold water inside the reservoir. Due to the density difference again the hot water rises inside the reservoir finally accumulating on the top portion of the reservoir and similarly cold water at the bottom. Thus stratification of the water depending on the temperature and density difference occurs inside the reservoir.

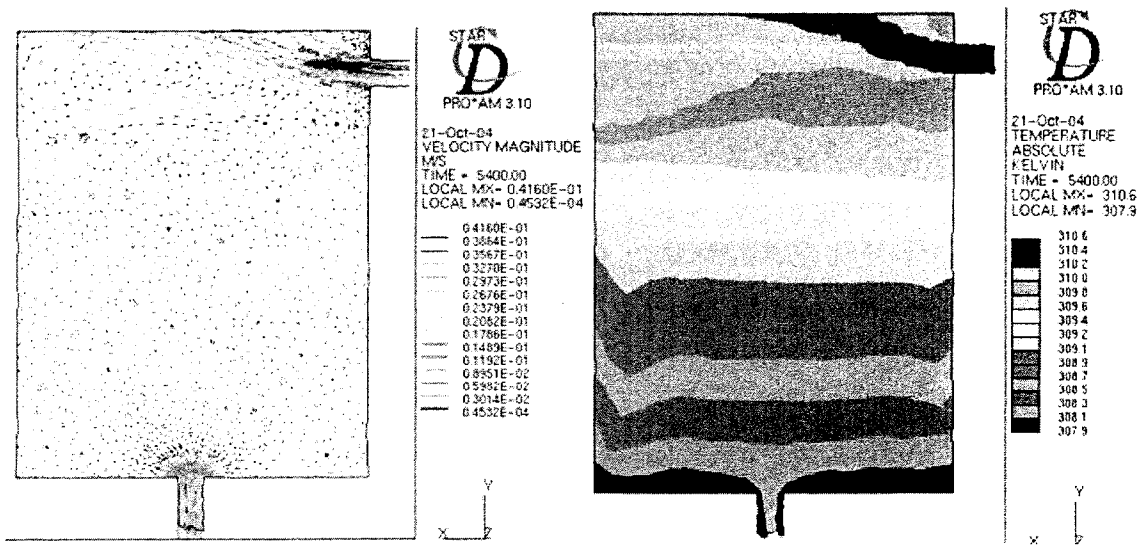

Figure 50: Velocity and temperature profile of water reservoir after 1.5 hours in real time

Figure 51 and 52 shows the velocity and temperature profiles inside the water reservoir after 12.22 hours of real-time simulations. It can be observed that there is rigorous mixing of water coming from the solar collector and the water inside the reservoir. The temperature inside the tank is observed to be constant which may be due to the fact that the temperature difference inside the water reservoir is extremely small to differentiate the exact values. Due to the fact that we simplified the problem so that all the boundary conditions are adiabatic except the solar collector surface, the values of temperature are extremely high as compared to a realistic solar water heater.

It can be observed that though there is some local high and low temperature zones inside the tank that is because the nature of flow inside the water reservoir, But besides this it can be seen that the hot water is located in the top layer of the reservoir.

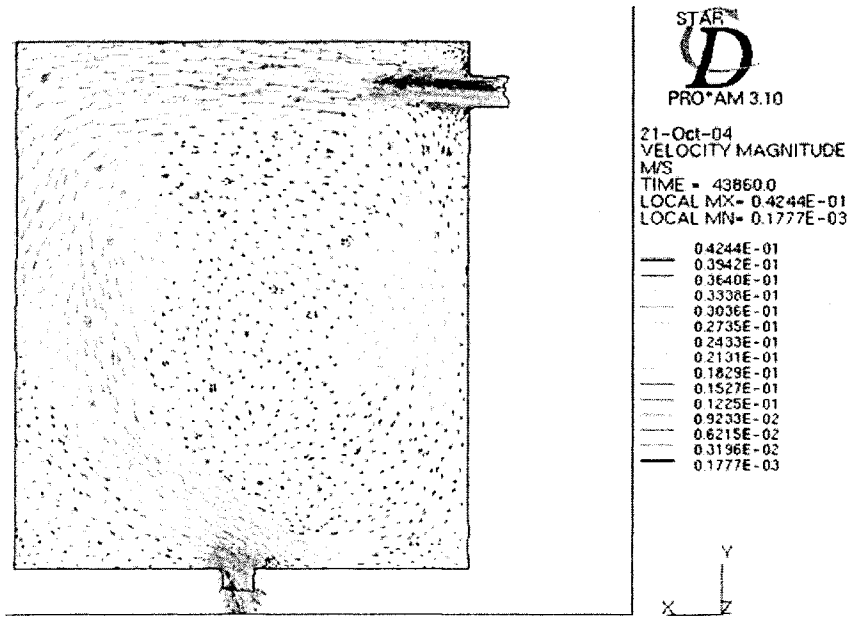

Figure 51: Velocity profile of closed loop solar water heater approximately after 12.22 hours in real time

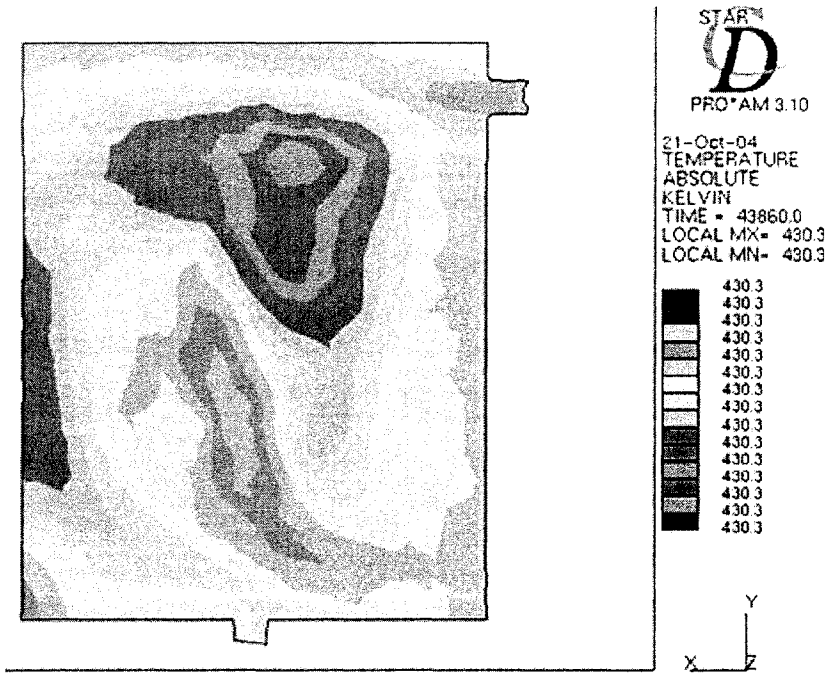

Figure 52: Temperature profile of closed loop solar water heater approximately after 12.22 hours in real time

Closed loop solar water heater performance was compared at 10:30 am with/without considering heat loss from solar collector. Figures 53, 54, 55 and 56 show the velocity and temperature profiles of the closed loop solar water heater for without and with considering the heat loss respectively. It can be observed that there is small difference in maximum velocity for the two cases which is due to fact of intruding the source momentum in the flow loop that simulates as pump. The maximum velocity in system is in the case where we do not consider the effect of heat losses. It is due to the fact that higher the temperature difference inside the bottom of the water reservoir and the top of the solar collector the effect of Boussinesq approximation is greater for this case as compared to the other case where we do consider the effect of heat loss. But as we are running the forced convection the effect of Boussinesq approximation will be very small or negligible, for the case of higher Reynolds number, on the performance of the forced convection solar water heater.

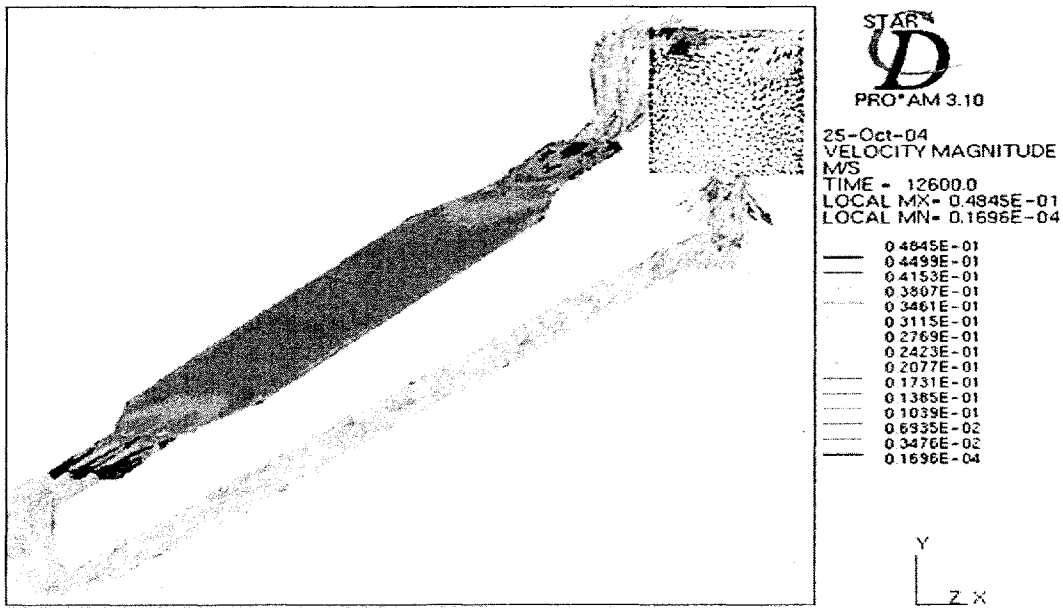

Figure 53: Velocity profile of closed loop solar water heater after 3.5 hours in real time without heat loss

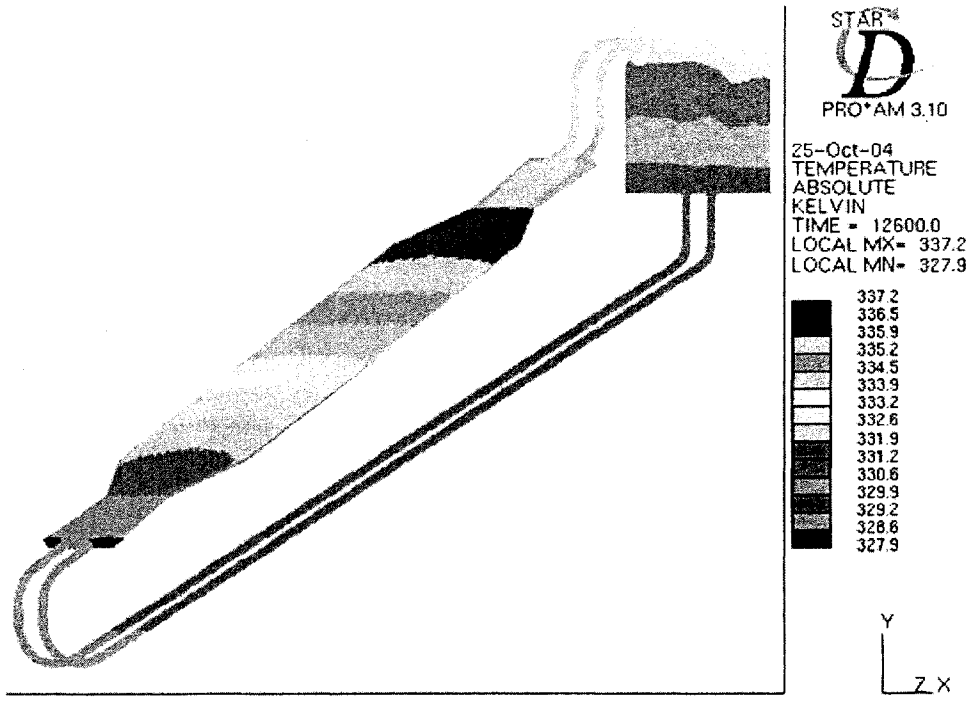

Figure 54: Temperature profile of closed loop solar water heater after 3.5 hours in real time without heat loss

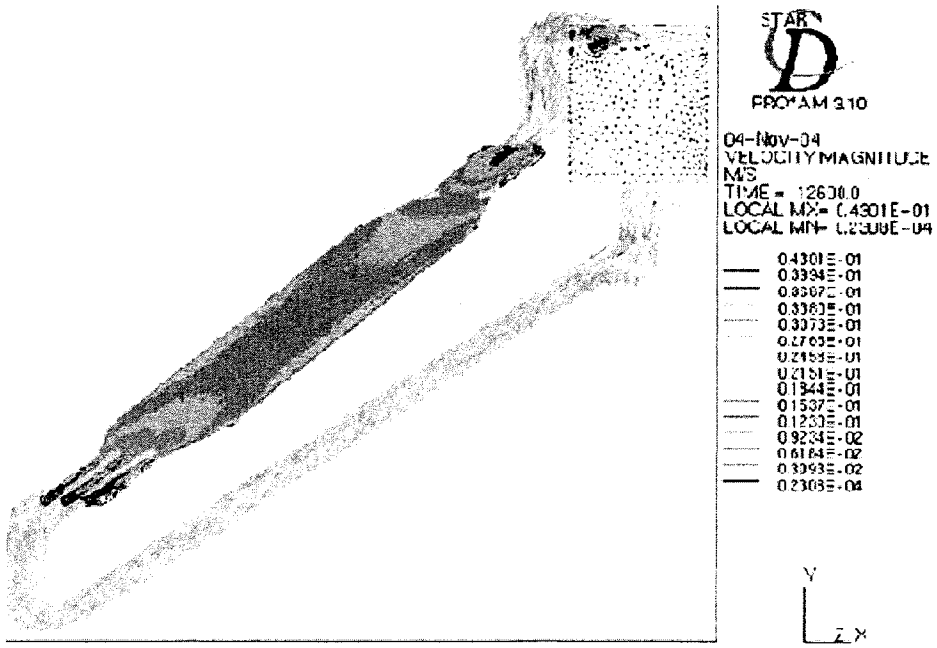

Figure 55: Velocity profile of closed loop solar water heater after 3.5 hours in real time with heat loss

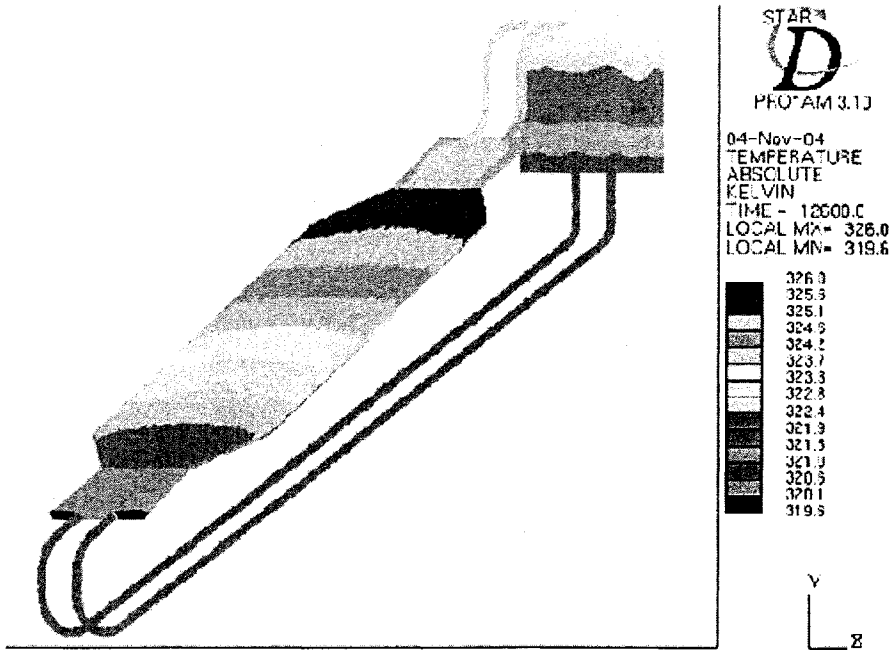

Figure 56: Temperature profile of closed loop solar water heater after 3.5 hours in real time with heat loss

From Figures 57 and 58 it can be observed that the shape of the velocity and temperature profiles for the two cases is same. From the temperature profiles it can be seen that the temperatures at the bottom and top of the collector as well as temperature difference between the top and bottom of the collector is greater for the case where no heat losses are considered.

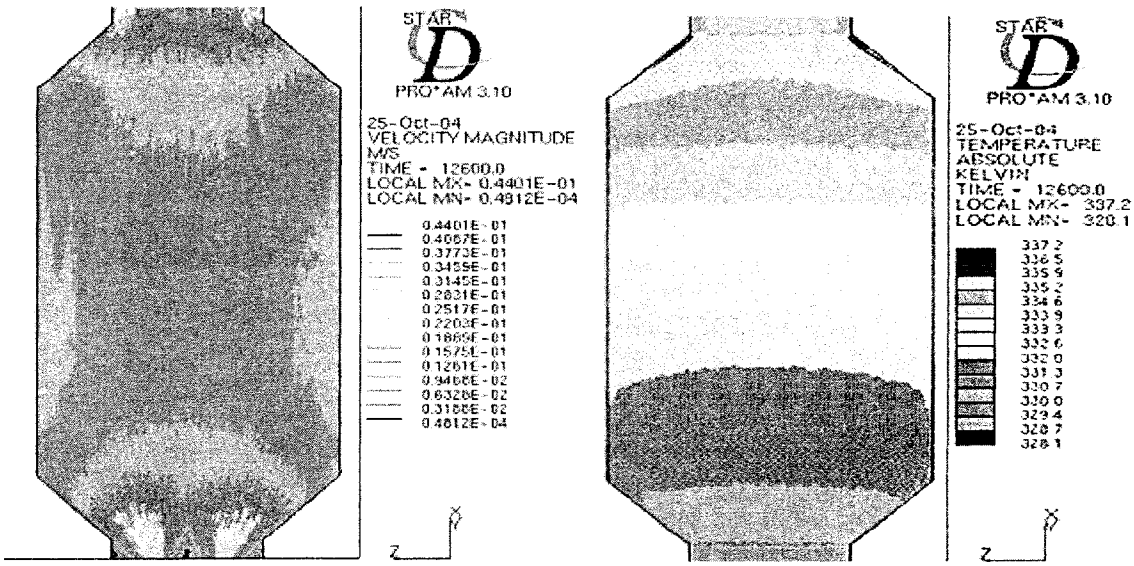

Figure 57: Velocity and temperature profile of solar collector after 3.5 hours in real time without heat loss

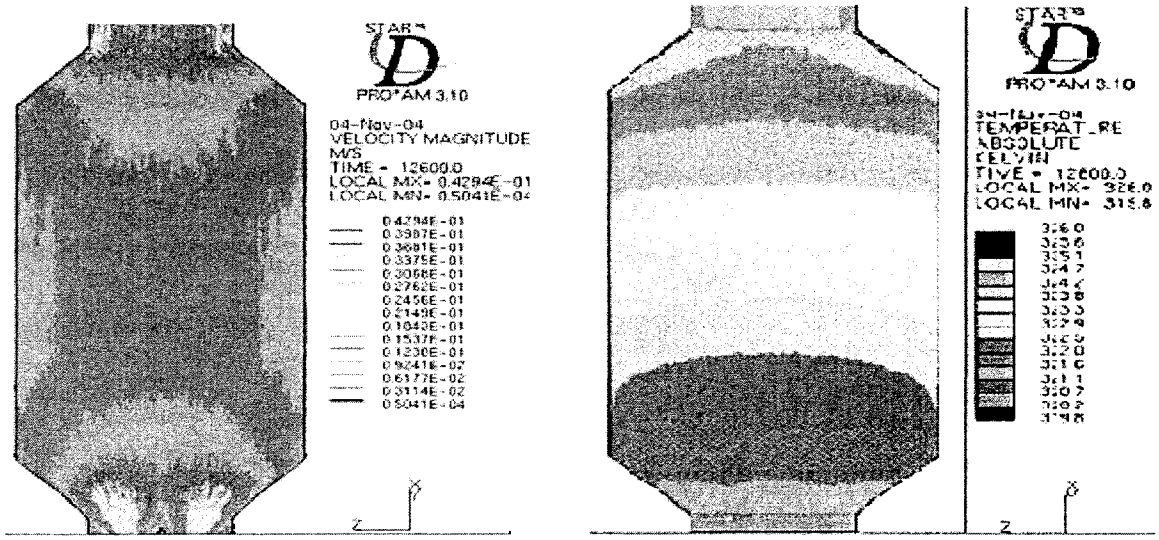

Figure 58: Velocity and temperature profile of solar collector after 3.5 hours in real time with heat loss

From Figures 59 and 60 it can be observed that there is a temperature of water at entrance and exit of the reservoir is greater for case in which we do not consider the heat loss.

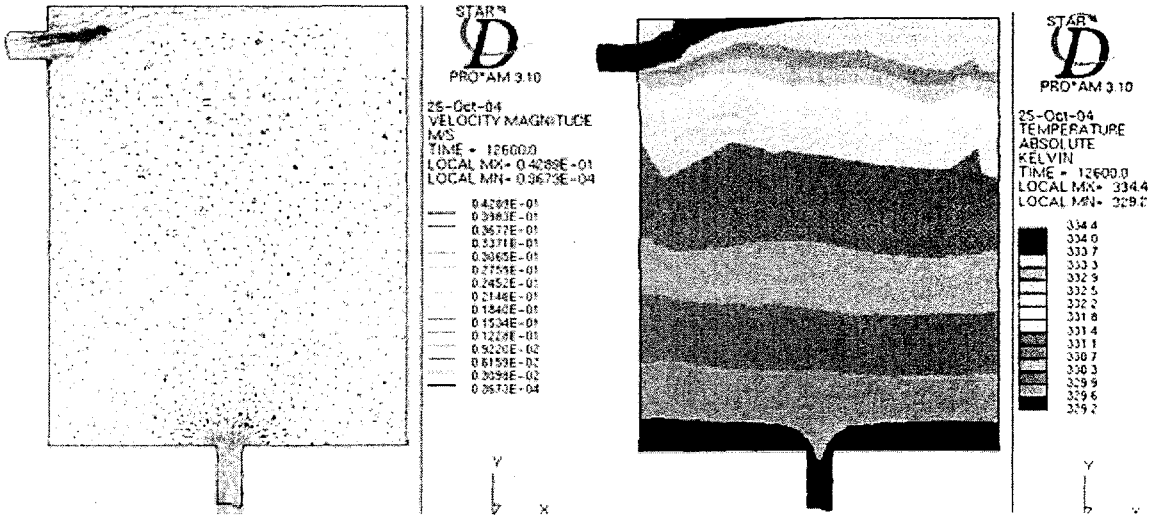

Figure 59: Velocity and temperature profile of water reservoir after 3.5 hours in real time without heat loss

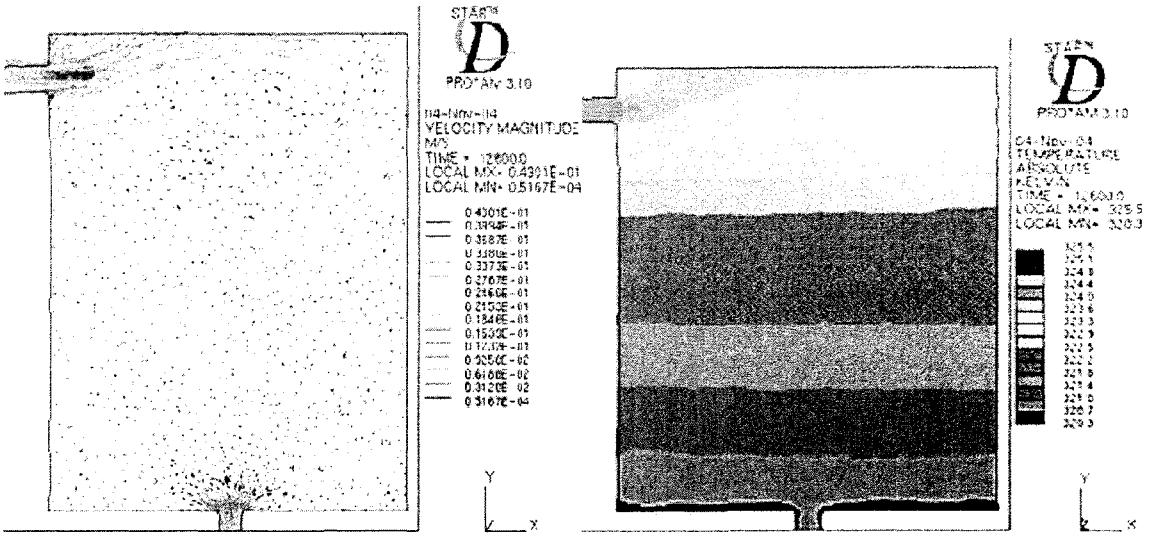

Figure 60: Velocity and temperature profile of water reservoir after 3.5 hours in real time with heat loss

3.1.2. Simulation data at 1000 Reynolds Number

Figure 61 and 62 shows the velocity and temperature profiles of the solar water heater. From the temperature profile it can be observed that the maximum temperature for the overall system at 1000 Reynolds number and minimum temperature for overall system is greater and lower as compared to the overall system at 1500 Reynolds number. This is due to the fact that the maximum velocity of water flowing inside the collector as well as overall system is lower for system in this case. Due to which the time for which water is in contact with collector is greater for case 2 as compared to case 1. Hence the heat gained by water is greater in case 2 as compared to case1.

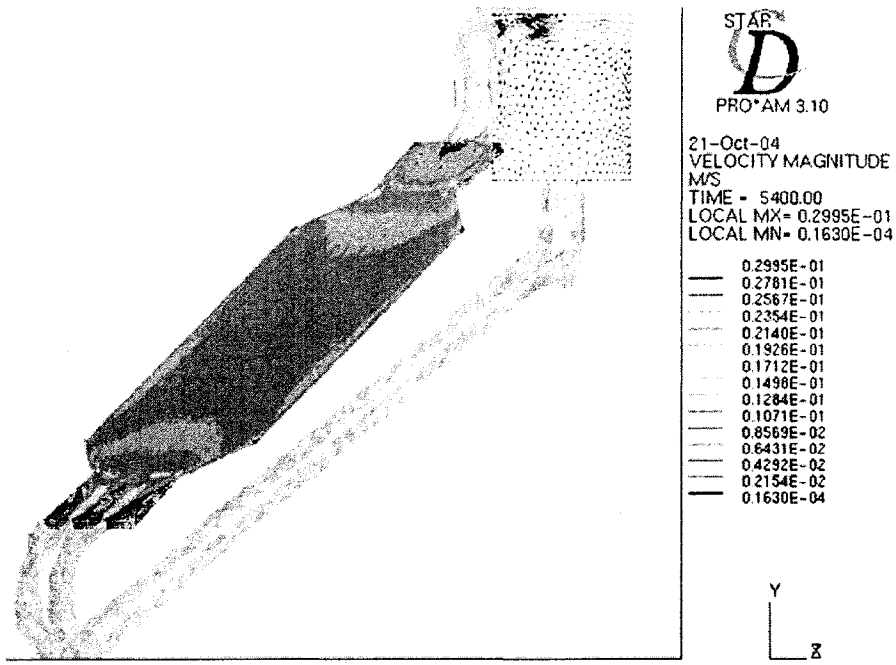

Figure 61: Velocity profile of closed loop solar water heater after 1.5 hours in real time

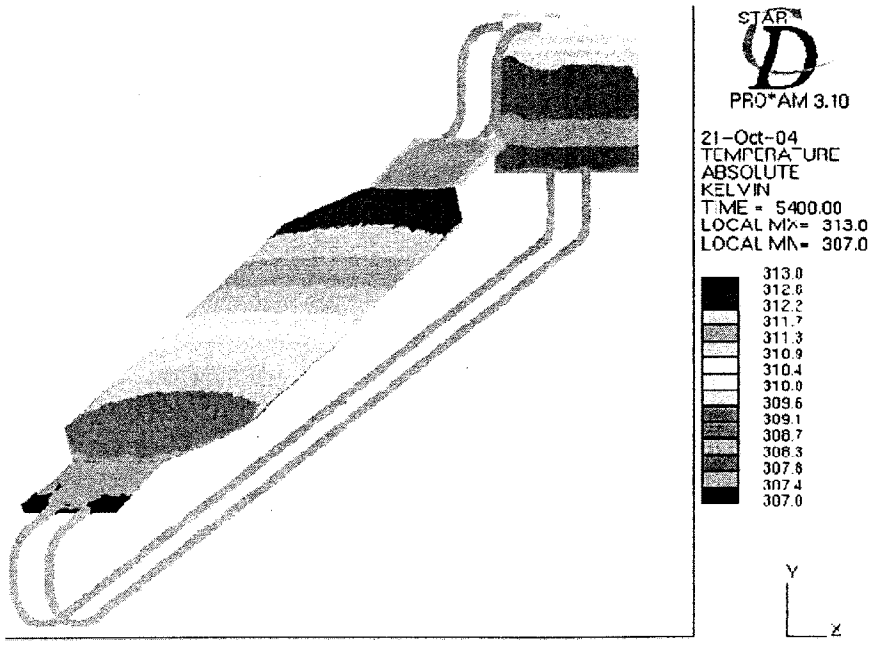

Figure 62: Temperature profile of closed loop solar water heater after 1.5 hours in real time

Figure 63 shows the velocity and temperature profile for the solar collector. It can be observed that the temperature difference across the solar collector for this case is greater than the case of 1500 Reynolds number. Which depicts that heat gain is greater for this case as compared to the case of 1500 Reynolds number.

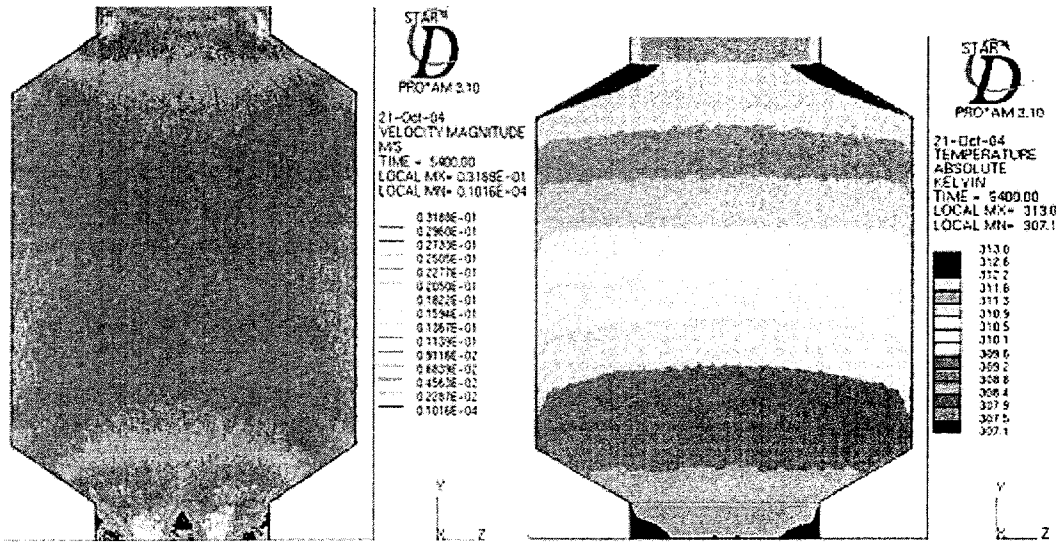

Figure 63: Velocity and temperature profile for solar collector after 1.5 hours in real time

Figure 64 shows the velocity and temperature profiles of the water reservoir. It can be observed that the water entering at higher temperature inside the reservoir starts moving upwards after entering and then moves down after reaching the opposite end. And hence mixes with the relatively cold water inside the reservoir and then rises inside the tank resulting in stratification of water according to the temperature.

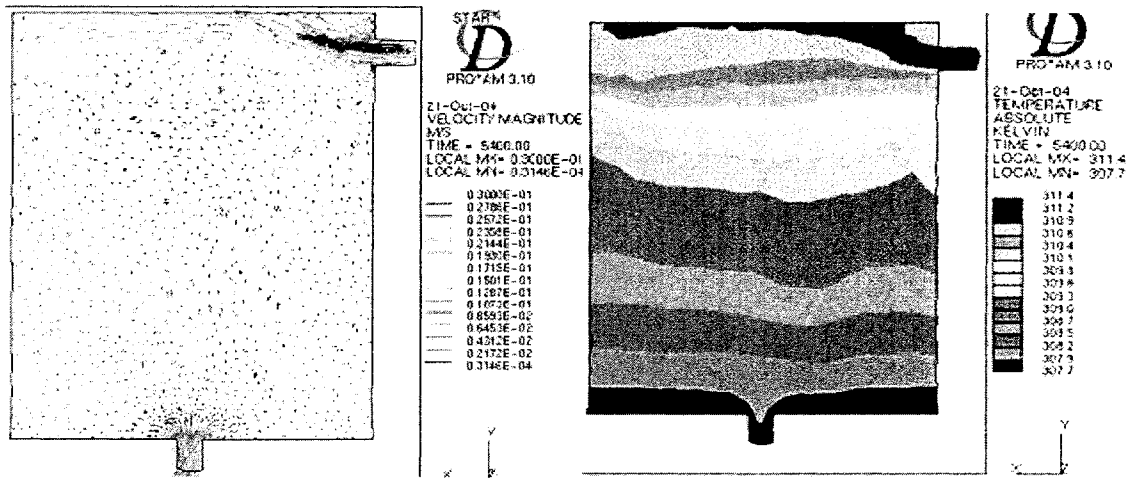

Figure 64: Velocity and temperature profile for water reservoir after 1.5 hours in real time

Figure 65 shows the velocity and temperature profile of the water reservoir after the 12.22 hours real-time simulation. The mixing can be clearly observed in the velocity profile. Even though there is not significant difference in temperature inside the water reservoir. It can be observed that there are some local zones inside the reservoir where the temperature is higher and lower with respect to rest of the reservoir temperature.

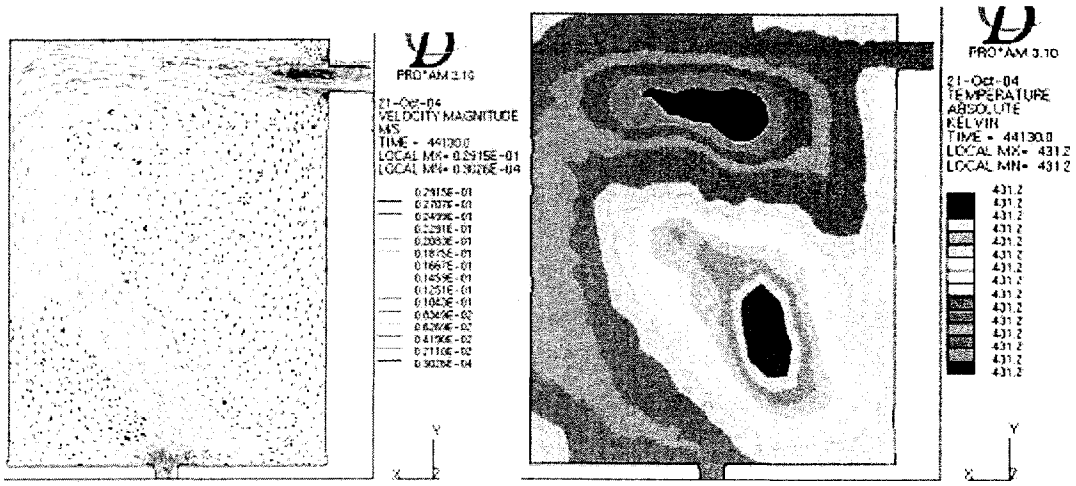

Figure 65: Velocity and temperature profile for water reservoir after 12.22 hours in real time

3.1.3. Simulation data at 500 Reynolds Number

Figure 66 and 67 shows the velocity and temperature profiles. It can be observed that maximum temperature for the over all system is greater for this case as compared to case 1 and case 2. The temperature difference is also high as compared to other two cases. Again the reasoning is same that as the system operates at lower Reynolds number than other two cases, the heat gain from the collector is greater as the water is in contact with the solar collector for maximum time.

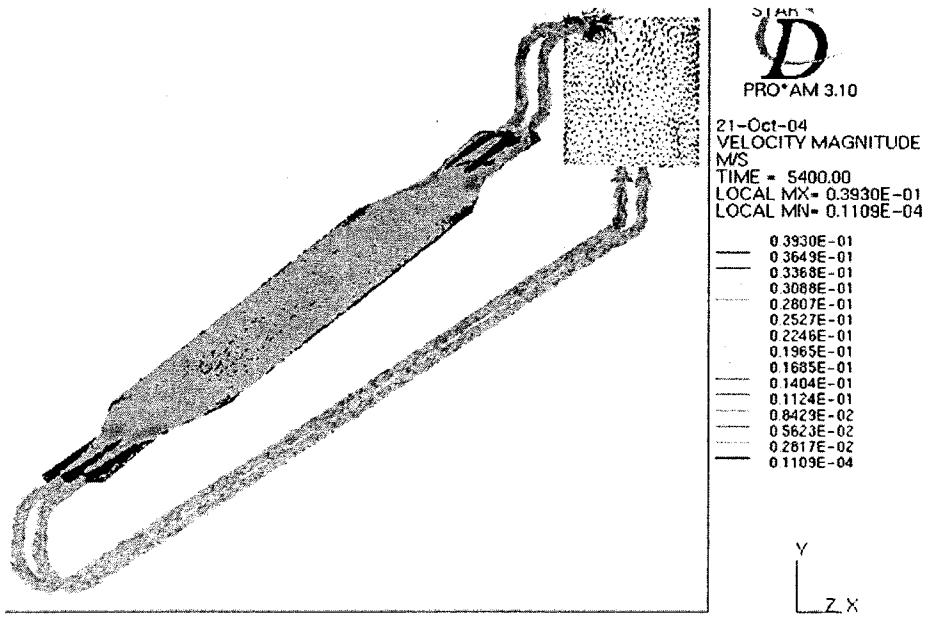

Figure 66: Velocity profile of closed loop solar water heater after 1.5 hours in real time

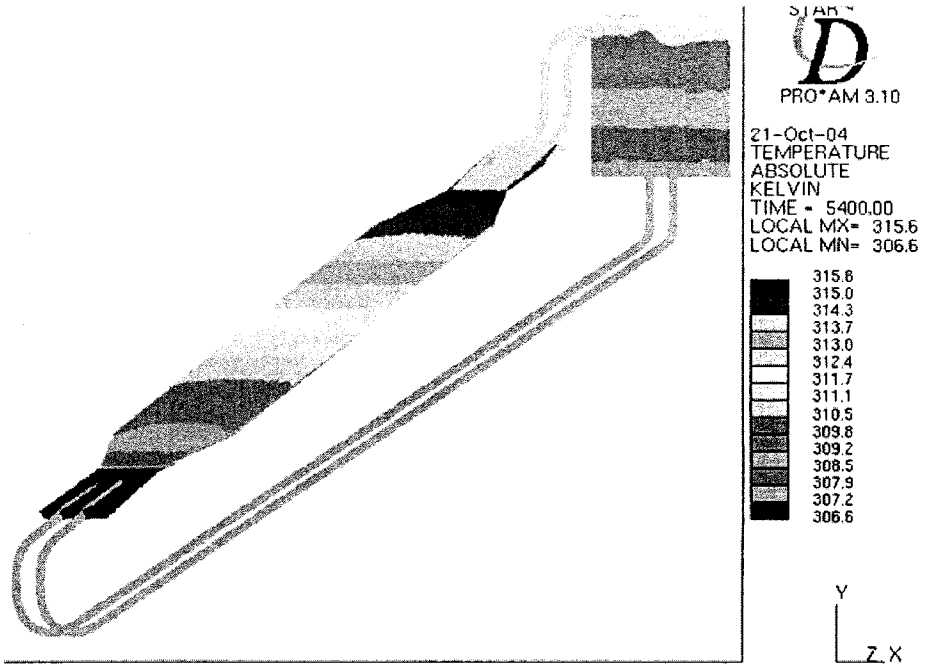

Figure 67: Temperature profile of closed loop solar water heater after 1.5 hours in real time

Figures 68 and 69 show the velocity and temperature profile inside the solar collector and reservoir. It can be observed that the temperature difference across the solar collector is greater than other two cases which results in higher heat gain as compared to other two systems.

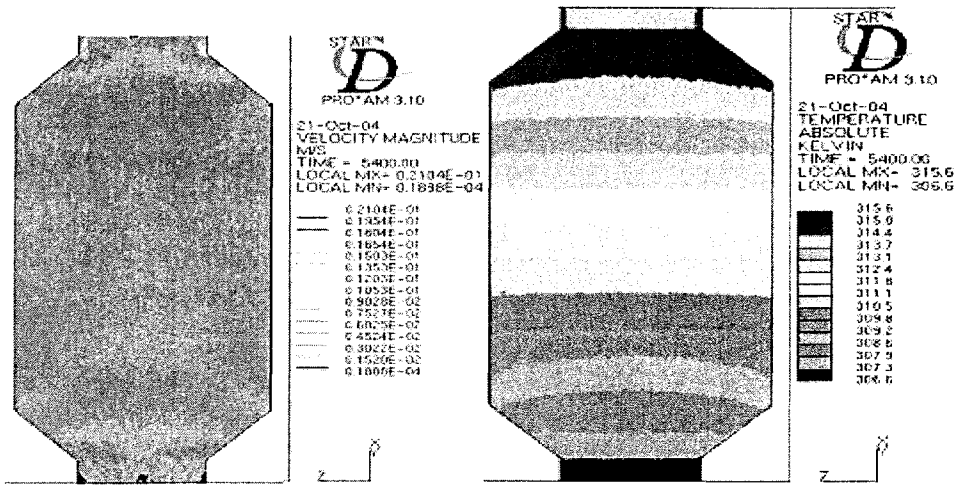

Figure 68: Velocity and temperature profile for solar collector after 1.5 hours in real time

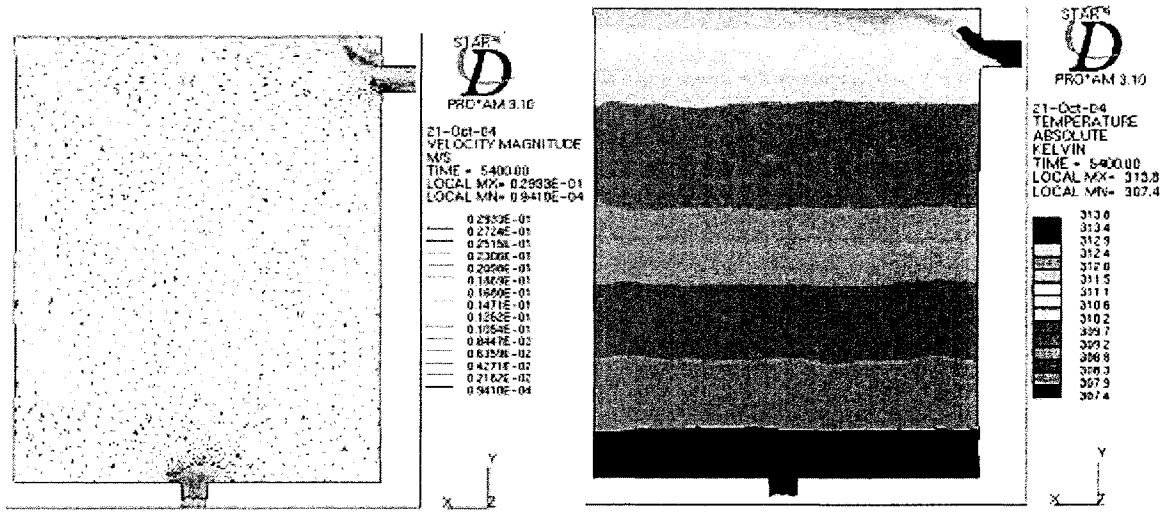

Figure 69: Velocity and temperature profile for water reservoir after 1.5 hours in real time

Figure 70 shows the velocity and temperature profiles of the water reservoir after 12.22 hours of real-time simulations. After 12.22 hours of real-time simulations from all the three cases of Reynolds number namely 1500, 1000 and 500 it can be observed that the maximum heat gain was obtained in case 3. Even though maximum velocity after two hours of real-time simulation for case 3 showed the higher value as compared to case 2, after 12.22 hours of real-time simulation the maximum velocity for case 3 was observed to be less than case 2. It can be also observed that this value of maximum velocity is observed neither inside the collector or the water reservoir. So this may happen due to the fact that after two hours of real-time simulation the mixed effect of natural and forced convection has resulted in greater maximum velocity as compared to the case 2 in which forced convection was still dominating after two hours of real-time simulation. This result can lead us to critical Reynolds number below which if the solar water heater system if operated may show a behavior of mixed convection.

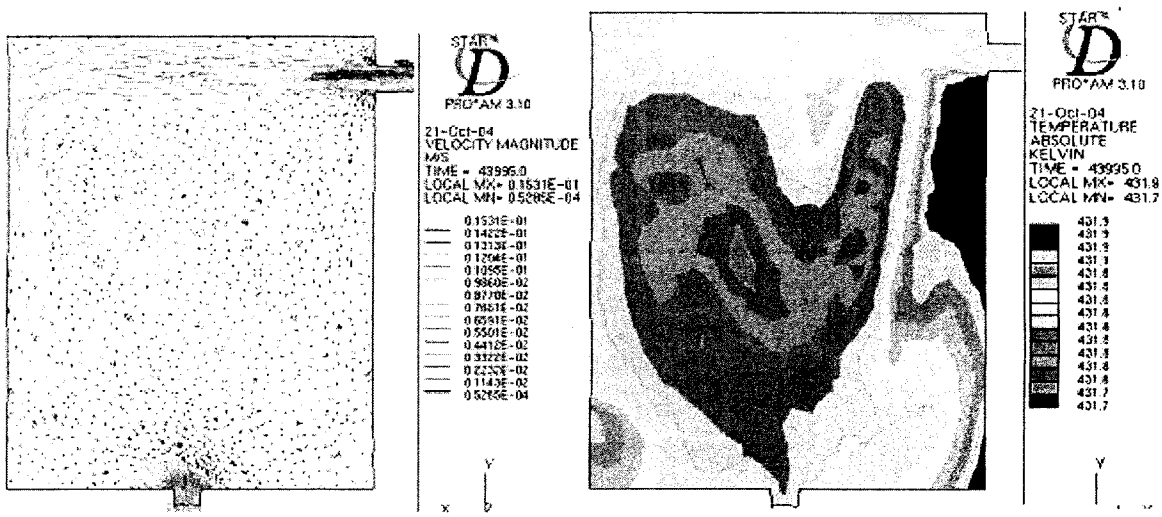

Figure 70: Velocity and temperature profile for solar collector after 12.22 hours in real time

Table 1. Comparison of results from Natural and forced convection cases at 1.5 hours

Forced Convection	Overall System		Collector		Reservoir	Mass Flow Rate
Reynolds Number	Max Temp	Min Temp	Max Temp	Min Temp	Mean Temp*	kg/sec
	deg K	deg K	deg K	deg K	deg K	
1500	312.1	307.4	312.1	307.8	309.25	0.2484
1000	313	307	313	307.1	309.55	0.1696
500	315.6	306.6	315.6	306.6	310.6	0.1121
Natural Convection**	313.3	305	313.3	307.1	309.8	0.2076

*Arithmetic mean was calculated

** Re for Natural case was found to be 557.63

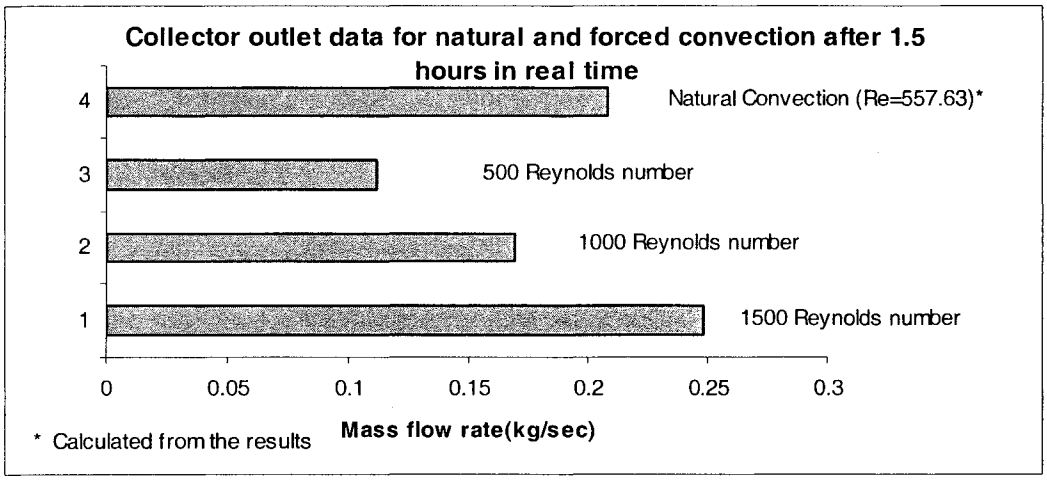

Figure 71: Mass flow rate at the collector top section for different cases

From the nature of model it can be observed that the natural convection system will act as a closed loop system till interval I of water usage. Table 1 shows the comparison of maximum and minimum temperatures obtained from the simulations after 1.5 hours in real time. It can be observed that as the Reynolds number decreases the temperature increases in the forced convection system. It can be observed that the forced convection case with 500 Reynolds number shows higher temperature behavior as

compared to the natural convection case which is due to the fact that the Reynolds number in the natural convection case was calculated from the simulation results and was found to be 557.63 at the same section where we force the momentum source inside the forced convection closed loop system. From figure 71 it can be observed that the mass flow rate for the natural convection case is greater than that of forced convection cases of 1000 and 500 Reynolds number.

CHAPTER 4

CONCLUSIONS AND FUTURE DIRECTION FOR RESEARCH

4.0. Conclusions

Literature review showed that there was numerous experimental and analytical works in this area of research but the work with CFD approach was very rare. For the proposed design for solar collector there is no experimental data for comparison of the simulated models. Numerical simulations were performed on Natural convection open loop system and forced convection closed loop system. The forced convection closed loop system was studied for three different Reynolds number. These simulations give valuable insight in the thermal behavior of the solar water heating systems. It was found from results that the heat gain increases with the reduction in Reynolds number. This behavior was similar to the one in literature [9]. It was also found from the results that the performance of forced convection case at 500 Re was found to be better than natural convection case after 1.5 hours in real time which was due to the fact that the Reynolds number in the natural convection case at that time was found from calculations to be 557.63.

The Numerical results for the behavior of temperature and mass flow rate inside the open loop natural convection system are compared with the reported experimental results and seems to have similar trend of behavior as the experimental results [22]. The

behavior inside the water reservoir also shows the mixing and stratification which is expected as mentioned in literature [2].

By and large, this study helped provide more insight into the thermal behavior of the solar water heating system. This could lead the way to simulating the next step where the realistic boundary conditions like heat losses can be coupled with the one used in present case. Eventually the insight gained from that simulation can pave the way to provide real design guidelines for improving the design and cost optimization of solar water heating systems to make it more efficient and economically feasible.

4.1. Future Work

- Study the numerical performance of closed loop forced convection case.
- Perform experiments to validate the numerical results for both natural and force convection case.
- Study the natural convection case to optimize the design for improving the performance of the system.
- Improve the numerical scheme for reducing the time involved in running the simulations.

REFERENCES

1. Mark P Malkin. Design of thermosyphon solar domestic hot water heater systems. 1985.
2. Myrna Dayan. High performance in low-flow solar domestic hot water systems. 1997
3. I.M. Michaelides and D.R. Wilson. Optimum design criteria for solar hot water systems. WREC 1996.
4. Adnan M. Shariah, Douglas C. Hittle and George O.G. Lof. Computer simulation and optimization of design parameters for thermosyphon solar water heater. ASME 1994.
5. I.M. Michaelides, W.C. Lee, D.R. Wilson and P.P. Votsis. Computer simulation of the performance of a thermosyphon solar water-heater. Applied Energy 1992.
6. B. Norton, J E J Edmonds and E. Kovolos. Dynamic simulation of indirect thermosyphon solar energy water heaters. Renewable Energy 1992.
7. M.F.M. Fahmy and Abd-El Sadek. Transient analysis of closed loop solar water heating system (effect of heat exchangers). Energy Conversion and Management 1990.

8. K. Chuawittayawuth, S. Kumar. Experimental investigation of temperature and flow distribution in a thermosyphon solar water heating system. Renewable Energy 2002.
9. Abdul –Jabbar N. Khalifa. Forced versus natural circulation solar water heaters: A comparative performance study. Renewable energy 1998.
10. M Hamdan. Simulation and experimental analysis of built in solar water heater. International Journal of Solar Energy 1995.
11. M. Issa, M. Al-Nimr. Temperature distribution inside hot water storage tanks of solar collectors. Journal of Solar Energy Engineering 1989.
12. M.Al-Nimr. Temperature distribution inside a solar collector storage tank of finite wall thickness. Transactions of ASME 1993.
13. Adnan M. Shariah and A Ecevit. Effect of hot water load temperature on the performance of a thermosyphon solar water heater with auxiliary electric heater. Energy conversion management 1995.
14. Eng. Malek Kabariti and Eng. Yaser Mowafi. Testing and evaluation of thermosyphon solar water heating system by means of components testing and whole system testing and simulation in Jordan.
15. I.M. Michaelides, D.R. Wilson. Simulation studies of the position of the auxiliary heater in thermosyphon solar water heating systems. Renewable energy 1997.
16. Soteries A. Kalogirou, Sofia Panteliou and Argiris Dentsoras. Artificial neural networks used for the performance prediction of a thermosyphon solar water heater. Renewable Energy 1999.

17. B. Norton, P.C. James, S.N.G. Lo. Alternative approaches to thermosyphon solar energy water heater performance analysis and characterization. Renewable and sustainable energy reviews 2001.

18. M. Altamush Siddiqui. Heat and fluid flow studies in the absorber tubes of a thermosyphonic solar water heater. AIAA-94-4098-CP.

19. Mohamed B. Gadi. Design and simulation of new energy-conscious system(CFD and solar simulation). Applied energy 2000.

20. STAR CD Methodology Manual.

21. National Renewable Energy Laboratory website http://rredc.nrel.gov/solar/old_data/nsrdb/hourly/1990/23169_90.txt

22. Todd N. Swift, Jeffery A Miller and Douglas C. Hittle. A systematic approach to improving thermosyphon SDHW model performance. Solar Engineering 1996, ASME 1996.

VITA

Graduate College
University of Nevada, Las Vegas

Sachin Sudhakar Deshmukh

Home Address:
4217 Cottage Circle, Apt#3
Las Vegas, NV 89119

Degrees:
Bachelor of Engineering, Mechanical Engineering, 1999
Anuradha Engineering College, Amravati University, India

Thesis Title:
3 D CFD Simulations of natural and forced convection solar domestic water heating systems

Thesis Examination Committee:
Chairperson, Dr. Samir Moujaes., Ph. D., PE
Committee Member, Dr. William Culbreth, Ph. D.
Committee Member, Dr. Mohamed Trabia, Ph. D.
Graduate Faculty Representative, Dr. Samaan Ladkany, Ph. D., PE